National Library of Canada
Bibliothèque nationale du Canada

Canadian Theses Service
Service des thèses canadiennes

Ottawa, Canada
K1A 0N4

NOTICE

The quality of this microform is heavily dependent upon the quality of the original thesis submitted for microfilming. Every effort has been made to ensure the highest quality of reproduction possible.

If pages are missing, contact the university which granted the degree.

Some pages may have indistinct print especially if the original pages were typed with a poor typewriter ribbon or if the university sent us an inferior photocopy.

Reproduction in full or in part of this microform is governed by the Canadian Copyright Act, R.S.C. 1970, c. C-30, and subsequent amendments.

AVIS

La qualité de cette microforme dépend grandement de la qualité de la thèse soumise au microfilmage. Nous avons tout fait pour assurer une qualité supérieure de reproduction.

S'il manque des pages, veuillez communiquer avec l'université qui a conféré le grade.

La qualité d'impression de certaines pages peut laisser à désirer, surtout si les pages originales ont été dactylographiées à l'aide d'un ruban usé ou si l'université nous a fait parvenir une photocopie de qualité inférieure.

La reproduction, même partielle, de cette microforme est soumise à la Loi canadienne sur le droit d'auteur, SRC 1970, c. C-30, et ses amendements subséquents.

NL-339 (r. 88/04) c

Canada

THE UNIVERSITY OF ALBERTA

REACTIVE SPUTTERING OF INDIUM NITRIDE

BY

KENNETH LLOYD WESTRA

(C)

A THESIS

SUBMITTED TO THE FACULTY OF GRADUATE STUDIES AND

RESEARCH IN PARTIAL FULFILMENT FOR THE DEGREE OF

MASTER OF SCIENCE

DEPARTMENT OF ELECTRICAL ENGINEERING

EDMONTON, ALBERTA

SPRING 1989

Permission has been granted to the National Library of Canada to microfilm this thesis and to lend or sell copies of the film.

The author (copyright owner) has reserved other publication rights, and neither the thesis nor extensive extracts from it may be printed or otherwise reproduced without his/her written permission.

L'autorisation a été accordée à la Bibliothèque nationale du Canada de microfilmer cette thèse et de prêter ou de vendre des exemplaires du film.

L'auteur (titulaire du droit d'auteur) se réserve les autres droits de publication; ni la thèse ni de longs extraits de celle-ci ne doivent être imprimés ou autrement reproduits sans son autorisation écrite.

ISBN 0-315-52819-2

THE UNIVERSITY OF ALBERTA

RELEASE FORM

NAME OF AUTHOR: KENNETH LLOYD WESTRA

TITLE OF THESIS: REACTIVE SPUTTERING OF INDIUM NITRIDE

DEGREE: MASTER OF SCIENCE

YEAR THIS DEGREE GRANTED: 1989

Permission is hereby granted to THE UNIVERSITY OF ALBERTA LIBRARY to reproduce single copies of this thesis and to lend or sell such copies for private, scholarly, or scientific research purposes only.

The author reserves other publication rights, and neither the thesis nor extensive extracts from it may be printed or otherwise reproduced without the author's written permission.

Ken Westra

5308 - 94 B Avenue
Edmonton, Alberta
T6B 0Z3

Date: Dec. 20/88

THE UNIVERSITY OF ALBERTA

FACULTY OF GRADUATE STUDIES AND RESEARCH

The undersigned certify that they have read, and recommend to the Faculty of Graduate Studies and Research for acceptance, a thesis entitled REACTIVE SPUTTERING OF INDIUM NITRIDE submitted by KENNETH LLOYD WESTRA in partial fulfilment of the requirements for the degree of MASTER OF SCIENCE.

M K Brett
.....
Supervisor

Douglas Lovey
.....

J W Anderdek
.....

Date: Dec. 19/88

To My Parents

Abstract

Thin films of indium nitride were deposited, for the first time, by reactive DC planar magnetron sputtering. These thin films were characterized using X-ray diffraction, scanning electron microscopy, bandgap analysis, Hall probe analysis, and Rutherford backscattering. The films were found to be n-type and degenerate with electron concentrations of 3 to 6×10^{20} cm^{-3} and electron mobilities from 5 to 10 cm^2/Vs. The bulk stoichiometry of the films, as measured by RBS, found the films to contain 10 to 11 atomic percent oxygen and to have an indium to nitrogen ratio of 1 ± 0.04. However, there was no clear evidence of an In_2O_3 or indium oxy-nitride phase.

From the characterization of InN, it is proposed that most of the oxygen is incorporated into the film by surface oxidation of the columnar growth structure after the film is removed from the system and exposed to air. Secondly, it is proposed that the low electron mobilities of the films are caused by ionized donor impurities, the source of which may be the small amount of oxygen incorporated into the film during sputtering.

The optical constants of these InN thin films were measured between 700 and 2700 nm using spectrophotometric techniques. The dielectric constant and the dominant scattering centre in the films were determined from the optical constants. The infrared reflectivity in the range 2.5 to 20 μm was measured and modelled using the Drude theory of free electrons. By fitting the modelled reflectivity to the measured infrared reflectivity, the electron effective mass was found to be 0.3 m_e.

ACKNOWLEDGEMENTS

I am deeply grateful to Dr. M.J. Brett, my supervisor, for his advice, encouragement, and never ending optimism for this research. I would also like to thank Graham McKinnon, Myriam Buchbinder, Glen Fitzpatrick, and Tom Smy for their support and encouragement, without which this thesis could not have been done. I wish to thank Dr. R.P.W. Lawson for the initial RBS measurements of the InN films and finally, I wish to thank the Alberta Microelectronic Centre for the financial support they provided during the course of this work.

TABLE OF CONTENTS

Chapter		Page
1	Introduction	1
	1.1 Previous work	2
2	Reactive Sputtering	5
	2.1 Thermodynamic Considerations	7
	2.2 Heats of Formation of InN	9
	2.3 Summary	10
3	Deposition	11
	3.1 Deposition Considerations	11
	3.1.1 Heat of Formation Analysis	11
	3.1.2 Target Excitation	12
	3.13 Maximum Target Power	13
	3.2 Deposition System	13
	3.3 Substrates and Substrate Cleaning	16
	3.4 Conditioning of the Sputter Chamber	17
	3.4.1 Residual Gases	17
	3.4.2 Reduction of the Residual Gas Concentration	18
	3.5 Deposition Conditions	22
	3.6 Summary	22
4	Characterization	24
	4.1 Structure	24
	4.1.1 Columnar Growth Structure	24
	4.1.2 X-Ray Diffraction	29
	4.2 Bandgap Determination	34

4.3 Resistivity and Film Thickness 39
4.4 Hall Probe Analysis 40
4.5 Rutherford Backscattering 42
4.6 Summary of the Characterization of the InN Films 44
5 Discussion of the Results 46
5.1 Stoichiometry of Other Nitrides 46
5.2 Oxygen Contamination 47
5.3 Low Electron Mobility 49
5.4 Summary 52
6 Optical Constants of InN 53
6.1 Measurement of the Optical Constants 54
6.1.1 Weakly Absorbing Region 56
6.1.2 Strongly Absorbing Region 59
6.1.3 Discussion 63
6.2 Dielectric Constant of the Lattice 66
6.3 Determination of the Dominant Scattering Mechanism 68
6.4 Infrared Reflectivity 68
6.4.1 Drude Theory of Free Electrons 70
6.4.2 Comparison Between the Modelled and Experimental Infrared Reflectivity 72
6.5 Mean Free Path 75
6.6 Summary 76
7 Conclusion 78
References 81
Appendix A Variation of the Electrical Properties with Deposition Conditions 91

LIST OF TABLES

Table	Page
2.1 Summary of the reaction classification scheme based on a heat of formation analysis.	8
2.2 Summary of the heats of formation calculation for InN.	10
3.1 The partial pressure of the residual gases in the sputter chamber before and after InN deposition.	19
3.2 Conditioning of the sputter chamber prior to sputtering.	21
3.3 Deposition parameters used to deposit 90 W InN film.	23
4.1 Identification of the XRD peaks of the InN film deposited at 90 W.	32
4.2 The bulk stoichiometry of the InN films as determined by RBS.	44
6.1 Determination of the dielectric constant of the lattice.	67
6.2 Various parameters of the InN films.	76
A.1 The bandgap of InN measured as a function of the target power.	94

LIST OF FIGURES

Figure	Page
3.1 Schematic diagram of the sputter system.	14
4.1 SEM fracture cross section of InN deposited on silicon.	26
4.2 Thornton zone model for columnar growth structures.	27
4.3 XRD spectra of the InN film deposited at 90 W.	30
4.4 A schematic diagram of a X-ray diffractometer	31
4.5 The square of the absorption coefficient near the band edge and the linear extrapolation used to determine bandgap.	36
4.6 The absorption near the band edge shows the presence of an Urbach tail.	38
4.7 RBS spectrum for the film deposited at 90 W.	43
5.1 The electron concentrations and mobilities of InN films reported in the literature.	50
6.1 Transmission spectrum of the InN film deposited at 90 W.	55
6.2 Transmission spectrum of the 90 W film in the weakly absorbing region.	58
6.3 The index of refraction (n) of the film deposited at 90 W film calculated using the two different techniques.	60
6.4 The extinction coefficient (k) of the film deposited at 90 W.	60
6.5 A schematic diagram of the transmission and reflection from a thin film/substrate stack.	62
6.6 The index of refraction (n) of the InN films deposited at 90 and 150 W.	64
6.7 The extinction coefficient (k) of the InN films deposited at 90 and 150 W.	64
6.8 The reported values of the index of refraction (n) of InN.	65
6.9 The absorption of the 90 and 150 W films and the power law (λ^m) fit to the data.	69
6.10 The measured and modelled infrared reflectivity of the film deposited	

at 90 W showing the fits to various electron effective masses. 73

6.11 The measured and modelled infrared reflectivity of the film deposited at 150 W showing the fits to various electron effective masses. 74

A.1 The Deposition rate of InN as a function of the target power. 92

A.2 Electron mobility and concentration as a function of the target power. 93

A.3 Electron mobility and concentration as a function of the sputter gas pressure. 95

List of Symbols

B	Magnetic field strength
B	Line width of the XRD peak
d	Film thickness
d	Interplanar spacing
DC	Direct current
E	Incident light energy
E_g	Bandgap
FWHM	Full width at half maximum
h	Planck's constant
I	Electrical current
k	Extinction coefficient
l	Mean free path
m_e	Mass of an electron
m^*_e	Effective mass of an electron
n	Index of refraction
n_e	Electron concentration
q	Charge of an electron
R	Total reflection
RBS	Rutherford backscattering
R_h	Hall coefficent
r_h	Scattering factor
r_m	Reflection from the mth interface
RF	Radio frequency
SEM	Scanning electron microscopy
t	Size of a crystallite

T	Transmission
T_{max}	Curve made from the transmission maxima
T_{min}	Curve made from the transmission minima
v_f	Fermi velocity
XRD	X-ray diffraction
α	Absorption coefficient
θ	Angle of the diffraction peak
θ_b	Bragg angle
ρ	Resistivity
λ	X-ray wavelength
λ	Wavelength of light
μ	Mobility
μ_h	Hall mobility
ε_∞	Dielectric constant of the lattice
$\varepsilon_1, \varepsilon_2$	Dielectric constants
γ	Reciprocal relaxation time
ε_0	Static dielectric constant
ω	Frequency of the incident light
ω_p	Plasma frequency

Chapter 1

Introduction

In recent years there has been a dramatic growth in the applications of solid state devices, placing great demands on available thin film materials. A desire to find materials that fill these needs has led to an intense research effort into the properties of many obscure compounds and semiconductors. Part of this research effort into new materials has been the deposition and characterization of indium nitride. Initially InN attracted attention because it is a member of the III-V group of semiconductors, which have become very important in electro-optics and high speed electronics. Although the research effort into InN has been very small, to date, compared to other materials, a number of important and technologically exciting properties have been reported. Indium nitride is a direct bandgap semiconductor, with the bandgap lying between 1.7 and 2.1 eV [1]. Until recently, the electron mobilities of the films were found to be quite low (< 100 cm^2/Vs) and films decomposed at a low temperature (620° C) [2]. These preliminary results had relegated InN to a research backwater, as compared to other III-V compounds. However, the recent work of Tansley and Foley (1984) [3,4] has shown that it is possible to deposit thin films of InN that have very high electron mobilities (4000 cm^2/Vs). This value compares well with the mobility of other technologically important semiconductors, such as GaAs which has a bulk electron mobility of 8800 cm^2/Vs [5], whereas the value reported for InN is for a polycrystalline thin film [6]. It is conceivable that the electron mobility of bulk crystalline InN could be as high as or higher than GaAs.

Since InN is a direct bandgap semiconductor, it could have electro-optic applications. However, it has not been studied in enough detail to identify possible applications in this field. The future potential of InN can be estimated by studying the properties of compounds closely related to InN. The closest related compounds to InN are the other

III-Nitrides: BN, AlN, GaN, and TlN. As thin films, GaN and AlN are the most studied of these compounds. AlN is used as a passivation layer in microelectronics [7], but has greatest potential as a piezoelectric thin film [8], and hence in electro-optic devices [9]. Recently, thin films of GaN have been successfully doped and made into a light emitting diode (LED) which emits light in the blue portion of the spectrum [10]. Perhaps the greatest potential of these III-N compounds lies in the alloying of them. AlN and GaN alloy together to form a compound that exhibits a direct bandgap which varies with composition [11,12,13]. Alloys of GaN and InN also exhibit similar bandgap variability [14,15] and some preliminary results suggest that this is also true for AlN/InN alloys [16]. The difference in size of the bandgap from AlN (5.5 eV) [9] to InN (1.7 eV) [17] may enable the production of LEDs and electro-optic devices that operate at any desired point in the spectral range from near infrared to ultraviolet.

It appears that there are many possible applications of the III-N group of semiconductors. In particular, InN has shown possibilities as an electro-optic material in alloys with GaN and AlN and for high speed electronic applications. However, the technological potential of InN has not been realized because of the difficulties in depositing material with the desired properties, particularly high electron mobilities. These problems must be overcome before the full potential of InN can be exploited.

1.1 Previous work

From its discovery in the 1940's [18], InN has been studied by only a small number of groups. In the last 20 years the basic properties of InN have been determined, though many properties have only been studied by a single group. The bandgap of InN is the most studied property and the literature has been reviewed by Tansley and Foley [1]. The effective mass of the electron has been determined from modelling of the infrared reflectivity using the Drude theory of free electrons and has been found to be 0.11 m_e

[19]. All of the studies of the carrier concentration and mobility of InN films have shown that all of the films are n-type with a majority having low electron mobilities (< 100 cm^2/Vs) and high carrier concentrations (10^{20} cm^{-3}) [19,20,21,22,23,24,25]. The films with mobilities greater than 100 cm^2/Vs fall into two groups: the high electron mobility films of Tansley and Foley (4000 cm^2/Vs) [3,4] and those with electron mobilities in the 100 to 250 cm^2/Vs range [26,27]. Since the mobility results of Tansley and Foley are so much greater than those of all other authors, a confirmation of their high electron mobility films should be a goal of future work with InN.

The optical constants of InN have not been studied in much detail, which is surprising considering how fundamental these constants are to understanding the material. The optical constants in the visible/near infrared region of the spectrum have been measured systematically by Tyagai et al. [19] and a number of groups have reported the index of refraction at specific wavelengths in this region [25,27]. The optical constants in the region above the bandgap (2.5 to 5.0 eV) have recently been determined using spectroscopic ellipsometry [28]. A number of band structure calculations for InN have been performed [29,30,31], but because the optical data for InN is so scarce it is difficult to judge the accuracy of these models.

As is the case for many materials that do not occur in nature, most of what is known about the properties of InN has been determined from thin film samples. Thin films of InN have been deposited using a number of different techniques such as reactive RF [4,24,27] and DC [14,19,22,25] diode sputtering, activated reactive evaporation [21], and chemical vapour deposition [20], with reactive diode sputtering the preferred method. This thesis reports, for the first time, deposition of InN using reactive DC planar magnetron sputtering.

The aim of this work was to study the deposition of InN by reactive DC planar magnetron sputtering of an indium target in N_2, with the goal of depositing high mobility films comparable to those reported by Tansley and Foley. The secondary aims were to study the bulk stoichiometry of the films and to measure the optical constants, and by modelling the infrared reflectivity, to determine the electron effective mass.

The reactivity of indium with N_2 and the residual gases in the sputter system, along with the consequences of these reactions, are discussed in Chapter 2. The deposition system, the conditions under which the films were deposited, and the methods used to reduce the residual gas pressure in the sputter chamber are discussed in Chapter 3. The characterization of the films by X-ray diffraction, bandgap measurements, Hall probe studies and the stoichiometry of the film bulk are discussed in Chapter 4. In Chapter 5, the possible mechanisms causing the incorporation of significant amounts of oxygen are discussed, as well as methods of increasing the electron mobility. The optical constants in the visible and near infrared region are reported in Chapter 6, as well as modelling of the infrared reflectivity using the Drude theory of free electrons.

Chapter 2

Reactive Sputtering

The physical process that underlies sputter deposition of thin films is very different than the process involved in deposition by evaporation. Sputtering is the ejection of atoms from a surface which is bombarded by particles [32]. This ejection process is caused by a transfer of momentum from the bombarding particles to the surface atoms. In sputter deposition, a portion of this ejected material lands on the substrate, creating thin film growth. Since the sputter process is caused by a transfer of momentum and does not depend on the melting point or vapour pressure of a material, a wide range of materials that are difficult to deposit by evaporation may be sputtered.

In sputter deposition, the bombarding particles are usually ions created by a low pressure glow discharge [32]. A target made of the material to be deposited is used as the cathode of this glow discharge. The negative potential on the target, not only sustains the discharge but it also accelerates some of the ions in the plasma toward the target, imparting these ions with sufficient momentum to sputter the surface atoms of the target. In planar magnetron sputtering, the glow discharge is confined near the surface of the target by a magnetic field formed by placing magnets behind the target. This intense source of ions near the target surface dramatically increases the rate at which ions bombard the target. This increases the deposition rate, as well as reducing the ion and electron bombardment of the substrate [32]. These favourable characteristics have made planar magnetron sputtering a common industrial deposition technique.

Not only can thin films of metals and alloys be deposited by sputtering, but thin films of compounds can also be deposited. To deposit thin films of compounds, a number of different sputter techniques have been developed, the simplest of which is to sputter a

target made from the compound [33]. This technique has been successfully used to deposit some compounds but for many compounds it presents problems, particularly in achieving the desired stoichiometry of the films. This is because the sticking coefficients of the various elements of the compound, at the substrate, are usually very different. Typically, one of the elements is more volatile than the other and the deposited film will be deficient in this volatile element. To make the films stoichiometric, small amounts of the volatile element are added to the sputter gas. This technique has been used to deposit stoichiometric films of GaAs from a GaAs target [34], in which a small amount of arsenic was added to the discharge to overcome the arsenic deficiency in the films. The logical extension of this idea is reactive sputtering, in which a metal target is sputtered in a sputter gas that contains significant amounts of the nonmetallic component of the compound. The metal and the reactive gas which contain the nonmetallic element react to form the compound; hence the name reactive sputtering. This technique was developed to deposit metal oxides but it has also been used to deposit various nitrides, flourides, sulfides, and carbides [35], forming a class of materials that had not previously been studied as thin films.

To deposit InN thin films, reactive sputtering of an indium target in N_2 was chosen instead of sputtering from a compound InN target. This is primarily because a source of high purity bulk InN needed to make the target was not available. Even if InN targets were available, reactive sputtering from an indium target is more desirable because compound targets can have contamination problems. One major source of contamination is caused by air trapped in the target during processing, because compound targets cannot be cast in a vacuum, as metal targets can. Compound targets must be hot pressed or sintered together and during this process air can become trapped in pockets within the target [33]. When the compound target is sputtered these pockets of trapped air are exposed and cause contamination of the growing film. Because of this possible

contamination problem, most researchers avoid using compound targets for depositing compound films.

2.1 Thermodynamic Considerations

In reactive sputtering, the reactivity of the reactive gas with the metal target has a large effect not only on the resultant film properties, but also on the deposition conditions. By calculating the reactivity of the metal and the reactive gas, it is possible to make rough estimates of the initial sputter conditions and the resultant film properties. This can be useful in planning experiments.

From studies of the reactive sputtering of metal targets in N_2 discharges, Winters and Kay [36] have proposed three different classes of reactivity that can occur between the metal target and the nitrogen plasma. In the first class of reactivity, the metal chemisorbs nitrogen to form the nitride. In the second class the metal does not chemisorb nitrogen, but does form a nitride. In the third class the metal does not chemisorb nitrogen or form a nitride. This classification system can be generalized to other compounds by applying a simple heat of formation calculation [37,38] to the compounds that can form by reactions between the metal and the reactive gas. The heats of formation for most compounds are usually tabulated for equilibrium conditions and room temperature, not the highly non-equilibrium conditions found in a glow discharge. However, these can be used to give a qualitative feel for which reactions may occur. This heat of formation analysis can also be extended to the reactions between the metal and the residual gases in the sputter chamber and used to assess the possibility of film contamination by these gases.

Using the nomenclature of the heat of formation analysis, the first class of reactions is classified as those in which a spontaneous reaction occurs between the reactive gas and the metal. For compounds that is found to have this class of reactivity (class 1), the reactive sputtering of these compounds is characterized by target hysteresis effects, the

growth of stoichiometric films, and low deposition rates at high reactive gas concentrations due to compound formation on the target surface during sputtering [38]. Reactive sputtering of most oxides and many nitrides is characterized by this type of reactivity [38,39]. The heat of formation calculation for the second class of reactivity (class 2) shows the reaction between the metal and the reactive gas to be non-spontaneous, but the reaction between the metal and the atomic element in the reactive gas as spontaneous. Thus the compound must be formed by a reaction between the metal atom with atomic or excited reactive gas species, and the compound will not form unless these species are present. Compounds that form by this type of reactivity can be reactively sputtered because a glow discharge is a source of these nonthermal species. The dynamics of the sputter process and the resultant film properties are dominated by the concentration of these excited species in the sputter chamber. Deposition of compounds with this type of reactivity by reactive sputtering are characterized by the lack of target hysteresis effects and the growth of non-stoichiometric films. NiN [36], and InN are examples of compounds that form by this type of reactivity. The non-spontaneous reactions between the reactive gas and the atomic species with the metal are indicative of the third class of reactivity (Class 3). Table 2.1 summarizes this classification scheme for the three different types of reactions.

Classification	Reactive Gas Type	Reactivity
Class 1	Molecular form	Spontaneous
Class 2	Molecular form	Non Spontaneous
	Atomic form	Spontaneous
Class 3	Molecular form	Non Spontaneous
	Atomic form	Non Spontaneous

Table 2.1 Summary of the reaction classification scheme based on a heat of formation analysis.

2.2 Heat of Formation of InN

The reactivity of indium with N_2 will dominate the sputter conditions and resultant film properties of the InN films grown in these experiments, although the reactivity of indium with the residual gases in the sputter gas will affect the amount of non-metalic contamination in the films. In Table 2.2 the reactivity of indium with the sputter gas and the reactive residual gases in the sputter system are shown. These residual gases typically consist of oxygen, nitrogen, and argon from air leaks into the vacuum system and water vapour which outgasses from the walls of the system [40]. As can be seen from the table, the reactivity of indium and N_2 is not spontaneous, but InN will form in a reaction between indium and atomic or excited nitrogen; a class 2 reactivity. This confirms the statements made in the literature that indium does not chemisorb N_2. A number of authors have proposed that the low electron mobilities seen in most InN films are due to nitrogen vacancies [6,21,25], which have their origin in this lack of reactivity between the indium and N_2. This also implies that the deposition and film properties of InN are dominated by the concentration of the non-thermal atomic and excited nitrogen species in the discharge. Unfortunately, the concentrations of these species cannot be directly measured, but can only be inferred from the electrical characteristics of the discharge.

The heat of formation analysis for the residual gases in the sputter chamber shows that the reaction between indium and oxygen is a class 1 reaction and the reaction with water vapour, is a class 2 reaction. Thus, there is a possiblity of oxygen contamination of the growing film, from both O_2 and water vapour. However, the amount of oxygen contamination due to the water vapour will be much smaller because water vapour will only react with the indium if it has been excited by the discharge. To reduce the amount of oxygen contamination in the films, the residual oxygen pressure in the chamber should

be made as small as possible. The last reaction in Table 2.2 is the reaction between InN and O_2, which is a class 1 (spontaneous) reaction. This raises the possiblity that after the InN films are removed from the vacuum chamber and exposed to air, the surface of the InN film could react with the oxygen to form a surface oxide layer.

Reaction	ΔH_f	Reactivity
$In+N \rightarrow InN$	- 1.42 eV/atom	Spontaneous
$In+1/2N_2 \rightarrow InN$	+0.92 eV/atom	Non Spontaneous
$In+ O_2 \rightarrow In_2O_3$	-2.12 eV/atom	Spontaneous
$2In + 3H_2O \rightarrow In_2O_3+3H_2$	+1.57 eV/atom	Non Spontaneous
$2InN+3/2\ O_2 \rightarrow In_2O_3$	-1.10 eV/atom	Spontaneous

Table 2.2 Summary of the heats of formation calculations for InN. The heats of formation are found in references 26 and 41.

2.3 Summary

Using a heats of formation analysis, predictions can be made about some of the gross properties of the films, discharge dynamics, and possible film contamination. For reactive sputtering of InN from an indium target in a N_2 discharge, the heats of formation study shows that InN will only form when indium comes in contact with either atomic or excited nitrogen. This suggests that the InN films could be deficient in nitrogen. The same heats of formation study also suggests that the reaction of the residual oxygen in the sputter system with indium could cause significant oxygen contamination of the InN films.

Chapter 3

Deposition

The choice of deposition conditions used to deposit a thin film has a direct bearing on the success or failure of producing a film with the desired properties. When choosing the deposition conditions one must take into account the conditions which are monitored and controlled, such as the sputter pressure and the target power, as well as those which affect the film properties in an indirect way, such as the geometry of the sputter system and the temperature of the target surface.

To understand how these conditions affect the InN films, the deposition conditions are described here in some detail. As well, the reasoning behind the choice of these conditions is discussed. The important deposition considerations in making InN films are the reactivity of indium with the various impurities in the vacuum system, the choice of target excitation (either DC or RF) and the problems posed by the sputtering of a metal with a low melting point.

3.1 Deposition Considerations

3.1.1 Heats of Formation Analysis

The heats of formation analysis of the possible reactions that could occur in the growing film predicts that there could be two problems in growing stoichiometric InN thin films: the non-reactivity of indium with molecular nitrogen causing the films to be indium rich (sub-stoichiometric in nitrogen) and the reactivity of indium with molecular oxygen, which can cause oxygen contamination of the InN films.

To maximize the amount of atomic nitrogen in the discharge, N_2 was chosen as the sputter gas rather than an argon/N_2 discharge, which is often used in reactive sputtering

[38]. The mixed Ar/N_2 discharges were not chosen because the presence of argon would enhance the indium deposition rate while reducing the amount of atomic nitrogen available to the film. The high reactivity of oxygen with indium raises concerns about oxygen contamination of the growing film, resulting from reactions between the residual oxygen in the chamber and the sputtered indium nitride film. To reduce the possibility of oxygen contamination, the base pressure of the system was reduced as much as possible. In these experiments, the base pressure was reduced by first locating and repairing any air leaks in the vacuum chamber and secondly by conditioning the system, prior to sputtering, to reduce the amount of gas adsorbed on the walls of the vacuum chamber.

3.1.2 Target Excitation

The planar magnetrons used in the sputter system can be excited by either DC or RF power supplies. RF planar magnetron sputtering would have been preferable for the deposition of InN, because RF sputtering is known to have a larger glow discharge associated with it than DC sputtering [42], enabling the production of more atomic nitrogen near the growing film. However, preliminary results have shown that RF planar magnetron sputtering in our system creates serious problems. The RF plasma generates radio frequency interference (RFI), which causes some of the instrumentation on the system, particularly the capacitance manometer and the mass flow controllers, to malfunction. A second, more serious problem, is the contamination of the InN films by metals that are sputtered from other surfaces in the sputter chamber. Rutherford backscattering (RBS) and energy dispersive X-ray analysis (EDAX) showed the films to contain significant amounts of Al, Fe, and Ti contamination (2-5 at.%). This contamination of the film by other metals was felt to be unacceptable and with the additional problems created by the RFI, it was decided not to RF sputter. The films grown using DC planar magnetron sputtering show no evidence of metal contamination.

3.1.3 Maximum Target Power

During sputtering, the surface of a target can reach relatively high temperatures due to heating by the bombarding ions and beyond a critical target power the temperature of the surface of a target can exceed the melting point of the target material. For indium, which has a low melting point (165° C), this critical power can be quite low. If the surface of the target melts, it may flow into the vacuum chamber destroying the target and damaging the system. From past experience [43], other targets with erosion rings of size comparable to ours, melted when more than 340 W DC was applied. To avoid any accidental melting of the target surface of our indium targets, the maximum power to the target was set at 210 W. Although this limits the maximum deposition rate, it is felt that caution outweighed the risk, considering the cost of each indium target ($1100 US).

3.2 Deposition System

The sputtering system used for these experiments was built by High Vacuum Systems Inc. (HVS) of Mississauga Ontario. The system was installed and tested in late 1986 as part of this thesis work. The system consists of a large (37"x20"x16") stainless steel chamber with the deposition sources arranged around the substrate holder in a box configuration (Figure 3.1). The deposition sources available consist of two planar magnetron sources (Vac-Tek Fleximag 1), which use 5"x8"x1/4" targets, and an electron beam evaporation source, which was not operational during these experiments. The high vacuum pumping stack consists of a CTI Cryo-Torr 8 cryopump and a throttle valve. The pressures in the system are measured using an ion gauge and a residual gas analyzer (RGA) in the high vacuum range and a capacitance manometer (Baratron model 127) at sputter pressures.

A set of quartz heater lamps can be used to heat the substrates during deposition. They are mounted on the side of the chamber just below magnetron position #2.

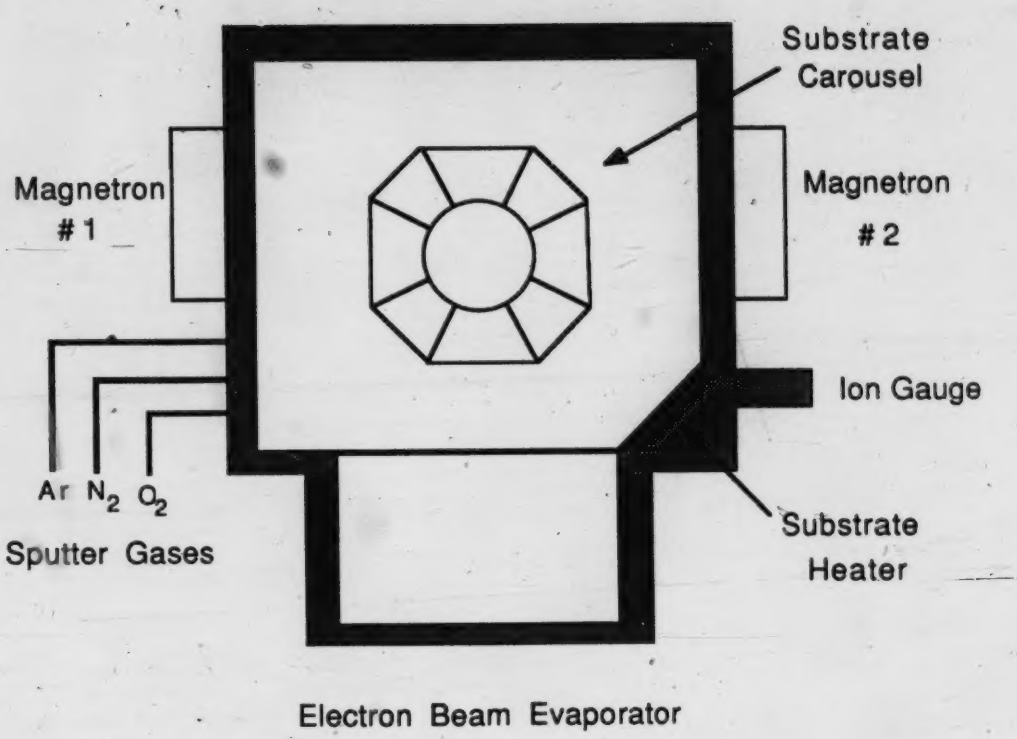

Figure 3.1 Schematic diagram of the sputter system. To simplify the diagram, the high vacuum pump is not shown.

Unfortunately, these lamps could not be used if magnetron #2 was also used because the sputter flux from the magnetron is deposited on the lamps. To protect the lamps from this sputter flux, they were covered with aluminium foil during all the experiments. This made it impossible to heat the substrates before or during deposition.

The system was 'baked out' (heated) prior to deposition to reduce the amount of adsorbed water vapour on the walls of the system. By decreasing the amount of adsorbed water vapour both the base pressure of the system and the amount of water vapour which is desorbed during sputtering is reduced. The heating of the vacuum chamber was performed using 1.2 kW heater tape that was installed on the outside surface of the vacuum chamber. The temperature of the interior of the system was monitored using a thermocouple that was attached to the substrate heater assembly inside the vacuum chamber. The amount of power delivered to the bake tape, and hence the chamber temperature, was controlled using a variac. The maximum internal temperature used to bake the system was 45° C, which corresponds to an outer chamber surface temperature of 70° C. This low temperature was chosen to decrease the possibility of damaging the O-rings as well as the indium target and seals.

The substrate holder consists of a carousel on which eight facets to hold the substrates are attached. A computer controlled stepper motor is used to control the motion of the substrate holder. The controller allows for the positioning of the facets in front of the deposition source and the rotation of the substrate holder. Two different sets of substrate facets were used in these experiments. For the first experiments, flat facets with clips to hold the substrates were used. Only three different films could be deposited per pump down sequence, because scattering of the sputtered flux by the sputter gas caused deposition at adjacent facets. For the later experiments, those reported in this thesis, each facet was equipped with its own shutter assembly that was moved in and out of position using a rotary push/pull feedthrough. Using this arrangement eight different films could

be deposited per pump down sequence. The disadvantage of this system was that the target/substrate distance could not be changed, due to alignment problems between the feedthrough and the shutters.

The planar magnetron targets can be powered by either DC or RF power supplies. The DC power supply used was an Advanced Energy 5 kW (MDX 5K) power supply. The RF supply is a Advanced Energy RFX 600 (13.56 MHz) supply and a 500 W matching network (ATN 500).

The nitrogen, which was used as the sputter gas, was quoted by the manufacturer as being 99.9998% pure. Two different indium targets were used in these experiments. The first target was a 5"x8"x1/4" 99.999 % pure indium target. This target was used in the early experiments as well as in those involving the screen discharge [17]. The second target was a 5"x8"x1/8" 99.999% pure indium target which was metallurgically bonded by the manufacturer to a copper backing plate. Films were deposited using both planar magnetron positions in the sputter chamber. There was no discernable difference in any of the properties of the films grown using either target, source, or target position.

3.3 Substrates and Substrate Cleaning

Typically each facet held four different substrates, a 1"x1"x0.04" quartz substrate, a Corning 7059 glass substrate with an edge masked by a microscope coverslip, a Corning 7059 glass masked by an aluminium shadow mask containing a hall probe pattern. The fourth substrate varied depending on which extra substrate was needed. For the RBS measurements a 1" diameter carbon disc was used.

The quartz substrate (Optosil 1) was used for the optical characterization experiments, since quartz is transparent to wavelengths as low as 200 nm and the optical constants for quartz are well known and tabulated in the range of interest (0.2 um to 20 um). The

1"x1" Corning 7059 glass with the masked edge was used both for thickness and resistivity measurements and for the X-ray diffraction studies. The Corning 7059 glass slide with the hall probe pattern was used to determine the carrier concentration and mobility of the films.

All of the substrates, except the carbon discs, were cleaned using a wet solvent cleaning technique before being placed in the deposition system. The cleaning process consisted of ultrasonic cleaning in methanol followed by a wash in deionized water, the substrates were then blown dry using dry nitrogen. Finally, they were individually wrapped in lens paper and stored until needed. This cleaning technique left no stains on the substrates and the films grown on these substrates contained few pin holes.

3.4 Conditioning of the Sputter Chamber

3.4.1 Residual Gases

From the heats of formation study and the initial deposition experiments of InN thin films, it was found that oxygen contamination of the film bulk was a serious problem. From this initial work, it was proposed that oxygen played a role in the low electron mobilities of the InN films [17]. Accordingly, to improve the quality of the InN films, the amount of oxygen in the films needed to be decreased. The oxygen content of the films can be reduced by either of two methods: increasing the deposition rate of InN or decreasing the residual oxygen concentration in the sputter gas. The low melting point of indium precludes a dramatic increase in the deposition rate, which leaves decreasing the residual oxygen concentration of the sputter gas as the other alternative.

Residual gases in a vacuum system consist of N_2, O_2, and Ar, which are caused by air leaks, and water vapour desorbed from the walls of the vacuum chamber. For pressures below 10^{-5} torr, the major constituent of this residual gas is typically water

vapour [44]. Water vapour is adsorbed onto the walls of the vacuum chamber whenever the vacuum chamber is exposed to air. In our chamber this occurs every time the system is opened to place new substrates into it. Since the amount of adsorbed water on the inside surfaces of the chamber exceeds the number of gas molecules present in the vacuum by orders of magnitude, the desorption of water vapour limits the speed at which the vacuum system will reach its ultimate base pressure [44]. The length of time needed to reach its ultimate base pressure can be reduced by accelerating the desorption process by heating the vacuum chamber.

One consquence of this 'outgassing' problem with our sputter system is that it takes over 24 hours for the vacuum chamber to reach the mid 10^{-7} torr range. This is largely due to the large surface area of the chamber and the inability to heat the chamber to high (>150° C) temperatures. Water vapour desorption from the walls of the vacuum chamber is further aggravated during sputtering because ion bombardment and heating occurs not only at the target and substrates, but also on all of the exposed surfaces in the chamber. It is not unusual to find that the residual water vapour pressure in the system after sputtering is an order of magnitude higher than it was prior to sputtering. This effect is described in Table 3.1, where the base pressure of the sputter system before and after a 5 hour deposition are shown. The measurements were taken 80 minutes after the end of the deposition, so that any water that had adsorbed onto the RGA head during deposition would be desorbed. Unfortunately, the sputter gas composition could not be monitored during sputtering.

3.4.2 Reduction of the Residual Gas Concentration

To reduce the base pressure of our sputtering system the vacuum chamber was leak-tested using a helium leak detector and any leaks that were found were repaired. The vacuum chamber was baked at 40°C for 15 hours and then allowed to cool to room

Prior to InN deposition:		
(Conditioned chamber)	1.2×10^{-7} torr	Base Pressure (ion gauge)
	7.4×10^{-9} torr	Oxygen partial pressure (mass 32)
	2.2×10^{-9} torr	H_2O partial pressure (mass 18)
After 5 hour InN deposition run:	8.5×10^{-7} torr	Base pressure (ion gauge)
	8.0×10^{-9} torr	Oxygen partial pressure (mass 32)
	6.0×10^{-8} torr	H_2O partial pressure (mass 18)

Note: 1) Throttle valve was in place for measurements.
2)The partial pressures were measured using the RGA and the partial pressures shown are the readings of the strongest peak in the gas' cracking pattern [ref. 40].

Table 3.1 The partial pressures of the residual gases in the sputter chamber before and after InN deposition.

temperature. Using these two simple techniques, the base pressure of the system was reduced from $3x10^{-6}$ torr to $1x10^{-7}$ torr.

To further decrease the base pressure and reduce the amount of adsorbed gas on the walls of the system, titanium was sputtered over the inside of the chamber prior to the deposition of the InN. A titanium target was placed in magnetron position #3 and sputtered in argon for 1 1/2 hours, while the substrate holder rotated in front of it. After this titanium sputter the base pressure of the system was $7.8x10^{-8}$ torr. With the present sputter system, this probably represented the lowest base pressure that could be achieved without modifying the system. Titanium was used because it acts as a getter pump, that is, it reacts with the residual reactive gases in the system to form stable titanium compounds [40]. The standard pump down procedure (chamber conditioning) used for these experiments, as well as the base pressures at various stages are shown in Table 3.2.

Before sputtering, the effective pumping speed of the cryopump in the chamber is reduced using a throttle valve. This is done because the high vacuum pumps do not operate at the high pressures needed for sputtering. One of the consequences of throttling is that the actual residual gas pressure during sputtering is not equal to the base pressure, but is a higher value, related to the amount of throttling of the cryopump. The base pressure with the throttle valve at the settings used during sputtering was $1.2x10^{-7}$ torr as opposed to $7.8x10^{-8}$ torr which is the quoted base pressure. Unfortunately, most authors quote only the base pressure of their chamber, not the pressure after throttling, which makes comparison of the residual gas content of the sputter gas reported by different authors, difficult.

To summarize, the residual gas content of a sputter gas is made up of contributions from a number of different sources. There are contributions from air leaks in the system, from water vapour that has desorbed from the walls of the chamber, and from the

1. Substrates loaded into the sputter chamber.

2. Pumpdown sequence begins.

3. Vacuum system is baked for 15 hours at 42° C (internal chamber temperature).

4. Sputter chamber is allowed to cool for 10 hours.

5. Sputter Titanium:
   - for 30 minutes
   - 400 W DC in 4.0 mtorr argon
   - substrate holder rotating at 5 min/rev

6. Wait for 1 hour.

7. Base pressure:
   - 9.8×10^{-8} torr (ion gauge)
   - 8.0×10^{-9} torr oxygen partial pressure (R.G.A. mass 32)
   - 1.8×10^{-8} torr water partial pressure (R.G.A. mass 18)

8. Proceed with InN deposition.

Table 3.2 Conditioning of the sputter chamber prior to sputtering.

throttling of the cryopump. For the most part the total residual gas content of the sputter gas is still quite small. The final base pressure of 7.8×10^{-8} torr is a good vacuum for most sputter applications and can be readily attained in this sputter system.

3.5 Deposition Conditions

Prior to deposition, the vacuum chamber was conditioned, as described previously, and films were not deposited until the base pressure of the system was at most 1.5×10^{-7} Torr. Just before the films were deposited and with the shutters closed, the indium target was presputtered in nitrogen for 30 minutes to remove any surface contamination from the target. The deposition conditions used to deposit the InN films are shown in Table 3.3. These conditions were chosen using the heat of formation analysis and deposition parameters typical for planar magnetron sputtering [38,39]. In this thesis, the variation of carrier concentration and the electron mobility of the films was measured as a function of deposition power and nitrogen gas pressure.

Although, the substrates were not intentionally heated during deposition, bombarding gas atoms and the deposited atoms do heat the substrate [32]. The substrate temperature was measured using a number of fixed melting point waxes. The temperature was found be approximately 100° C for the highest deposition power used (210 W DC).

3.6 Summary

Ideal sputter conditions for depositing stoichiometric InN would include an abundance of atomic nitrogen and a lack of oxygen in the sputter chamber. In practice, the atomic nitrogen concentration was maximized by using a pure nitrogen discharge and the oxygen content of the sputter gas was minimized by having as low a base pressure as possible. The base pressure was minimized by repairing the air leaks into the system and preconditioning the vacuum chamber by heating and presputtering of titanium.

1. Vacuum chamber conditioned (Bake and titanium presputter).

2. Base Pressure: 9.8×10^{-8} torr.

3. Target/substrate distance: 15 cm.

4. Indium target burn in:
   - Length of burn in: 30 minutes
   - Target Power: 90 w DC
   - Sputter gas pressure: 4.0 mTorr
   - Sputter gas flow rate: 20.5 sccm N_2

5. Deposition of the InN films:
   - 90 W DC (target voltage 412 V)
   - 20.5 sccm N_2
   - 4.0 mTorr
   - 33 minute deposition (1.0 μm film)
   - maximum substrate temperature 100° C

Table 3.3 Deposition parameters used to deposit 90 W InN thin film.

Chapter 4

Characterization

The InN thin films were characterized for various film properties such as structure, bandgap, and stoichiometry, as well as for the electron mobility and concentration. The structure of the films was studied using scanning electron microscopy (SEM) fracture cross sections and X-ray diffraction. The bandgap of the films was determined using optical absorption measurements near the band edge and the bulk stoichiometry of the films was measured using Rutherford backscattering analysis.

The results reported in this chapter are for a single set of experiments studying the effect of increasing deposition rate on the properties of the InN films. In particular, the characterization of one of these films, the film deposited at 90 W, is described in detail. During the course of my work, sixty eight sets of films were deposited. Of these sixty eight, the electrical properties of thirty seven and the bandgap of thirteen were determined. As well, the crystal structure of eighteen films was determined using XRD and finally the stoichiometry of ten films was measured by RBS. From this in depth study of the effect of variation of the deposition conditions on the properties of InN, it can be said with some confidence that the results presented in this chapter are representative of all the films deposited and studied in the last two years.

4.1 Structure

4.1.1 Columnar Growth Structure

The growth structure of thin films can be studied by either SEM studies of the film surface or SEM studies of fracture cross sections of the films. SEM fracture cross sections show that thin films typically consist of a columnar structure with voided regions between the columns [45]. This columnar structure is formed by the atomic shadowing of the incoming deposition flux by the previously deposited material or by irregularities on

the substrate surface. The fracture cross section of sputtered InN films (Figure 4.1) shows evidence of this columnar structure.

In the 1960's, Movchan and Demchisin published the first successful classification scheme of these columnar structures [46], which they called a 'structure zone model' (SZM), which was developed from their work with evaporated films. Although this classification scheme is only qualitative in nature, it does shed light on the processes that occur during deposition and on how these processes can affect the resulting film properties. The transition regions between different columnar structures are determined using the ratio of the substrate temperature to the melting point of the deposited material, which is a measure of the mobility of the adatom on the film surface. The first type of structure (zone 1) occurs at low substrate temperatures ($T/T_m<0.3$) and is characterized by large dome-like columns separated by large void regions (Figure 4.2). At these low temperatures, the deposited atoms 'stick where they land' and are not mobile enough to move into the voided regions which are shadowed by columns. Zone 1 films are not used in many applications because of the large void area around each column which can cause instability of the film properties with time due to oxidation of the column boundaries (film aging).

The second type of columnar structure (zone 2 , $0.2< T/T_m <0.5$) consists of a denser pack of smaller columns with smaller voided regions. The smaller void and columnar structure are due to the increased adatom mobility, since some of the adatoms are now mobile enough on the film surface to overcome the effects of shadowing and settle in the voided regions. At higher substrate temperatures, the third type of structure appears (zone 3, $T/T_m>0.7$). This structure is characterized by a lack of columnar structure and the obvious formation of grains. The limiting case of this type of structure is the growth of single crystal, epitaxial thin films. The very small void region and large grains of a zone 3 structure make these films desirable in many applications.

Figure 4.1 SEM fracture cross section of InN film deposited on silicon. This micrograph shows the columnar structure of the film.

Figure 4.2 has been removed because copyright permission for this figure has not arrived.

This figure was taken from:

J.A Thornton

"The microstructure of sputter-deposited coatings"

J. Vac. Sci. Technol. A 4 (6), 3059 (1986).

Figure 2

Unfortunately, the high temperatures involved in the deposition usually rule out their application in many traditional physical vapour deposition (PVD) film applications.

Thornton [45,47] has extended the Movchan and Demchisin SZM to sputtering by adding a third axis that takes the bombardment of the growing film by the sputter gas into consideration. This bombardment flux is another mechanism for adatom mobility [48], since the bombarding flux can sputter some of the growing film and redeposit it elsewhere on the film. This resputtering of the film during deposition shifts the transition temperature between the various zones to lower temperatures. As well, at certain temperatures and bombardment rates it also forms a completely new type of columnar structure, not seen in evaporated films, known as a zone T structure (Figure 4.2). This structure is a transition structure between zone 1 and zone 2. The film is characterized by a tight fibrous columnar structure with a small void area. The low temperatures associated with the deposition of zone T films and the small void area have made these films desirable in many applications, such as metallization in the microelectronics industry, solar coatings and decorative coatings on plastics. The major disadvantage of these films is that they are usually under tremendous stress [49].

To predict the columnar structure of a film requires the identification of the adatom which is mobile on the film surface. While for metals this is simple, for reactively sputtered thin films it isn't clear if the adatom is a metal atom or a molecule of the compound. For most reactively sputtered materials and deposition conditions the difference between the ratio of the substrate temperature to the melting point of the target material and the deposited compound is small. For these cases the identity of the adatom is not important in predicting the final film structure using SZMs. For example, for TiN deposited at 200° C, the T/T_m for Ti is 0.24 and for TiN it is 0.15, which implies a zone 1 or zone T structure depending on the bombardment rates. However, for InN the zone assignment is difficult because of the large difference between the melting point of indium

(165° C) and InN (1430° C). The substrate temperature during the deposition of InN was at most 100° C and, assuming the adatom is indium, a zone 3 structure would result. If, on the other hand, the adatom is InN, then it should form a zone 1 or T structure. Since the identity of the adatom in our depositions is not known and furthermore, it could change with the deposition conditions [6], the columnar structure of InN can not be predicted. The SEM fracture cross section of the InN film, Figure 4.1, shows a dense columnar structure, which cannot be readily classified using the SZM.

4.1.2 X-ray Diffraction

Generally, thin films can have a wide range of crystal structures, the two extremes being amorphous and single crystal films. Most thin films consist of a mixture of these two extremes, that is, polycrystalline with amorphous regions [50]. The crystal structure of thin films can be readily identified by X-ray diffractometry (XRD), this also provides information on stresses in the film, crystallite orientation and size.

The crystalline structure of the InN thin films was determined using X-ray diffractometry (XRD) of the as-deposited films on 7059 glass substrates, not powdered samples. Initial measurements were made in the Department of Metallurgy with CuKα radiation, while later measurements were performed using the diffractometer in the Department of Geology with CoKα radiation. An XRD spectrum for an InN film deposited at 90 W is shown in Figure 4.3; this spectra was taken using CoKα radiation. The peaks in the spectrum are due to diffraction from various crystallites in the film.

The interplanar spacing, the d-spacing, of the diffracting crystallites in the film were determined from Bragg's law [51]:

$$\lambda=2d\sin(\emptyset) \qquad (4.1)$$

Figure 4.3 XRD spectra of the InN film deposited at 90 W.

Measurement taken using Co Kα radiation

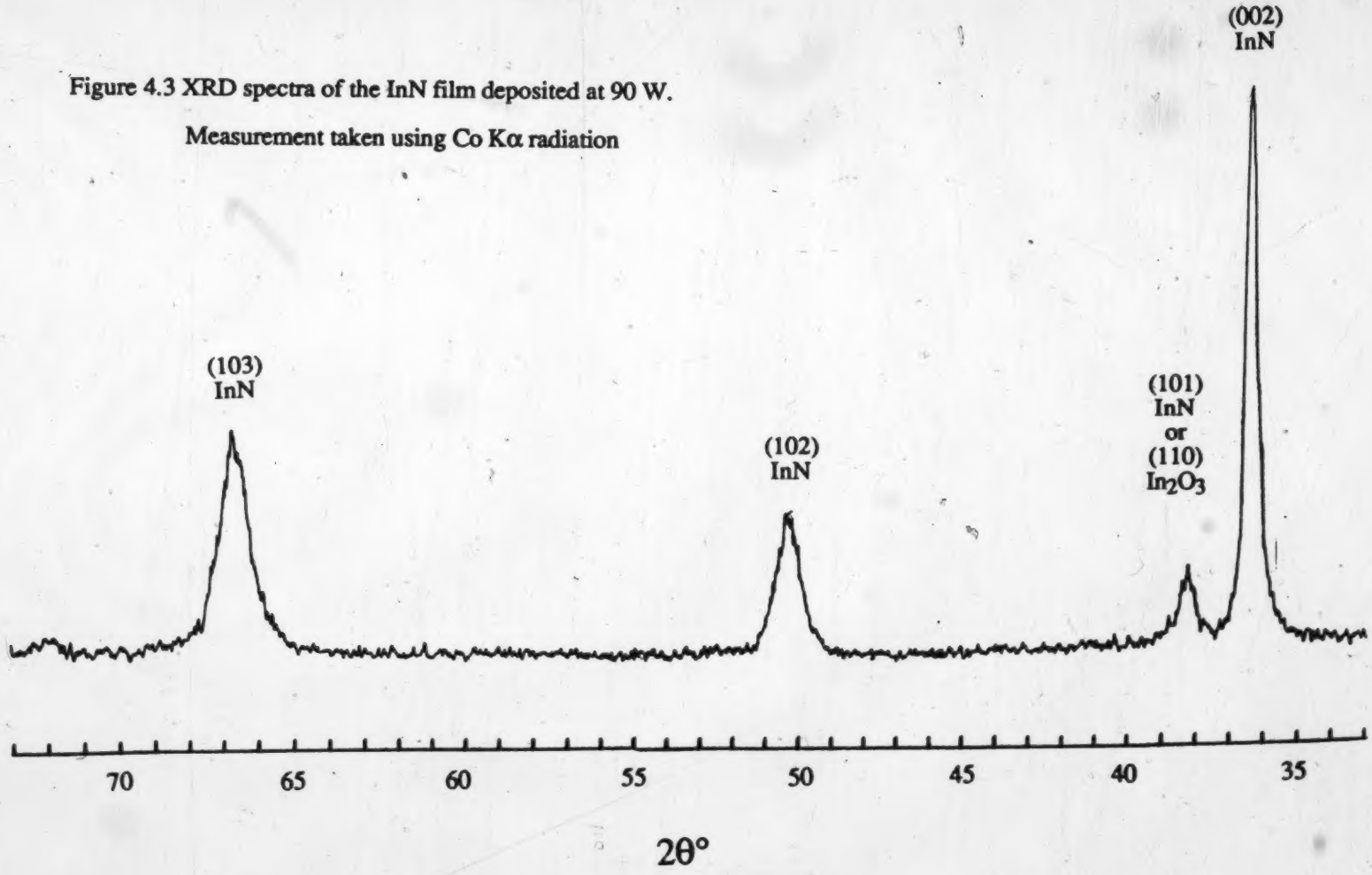

where: λ is the wavelength of the x-rays used, Ø is the position of the diffraction peaks and d is the interplanar spacing. As shown in Figure 4.4, the position of a diffraction peak, as determined by the diffractometer, is 2Ø, not Ø and this difference must be accounted for when calculating the interplanar spacings. Table 4.1 shows the interplanar spacings of the crystallites seen in Figure 4.3.

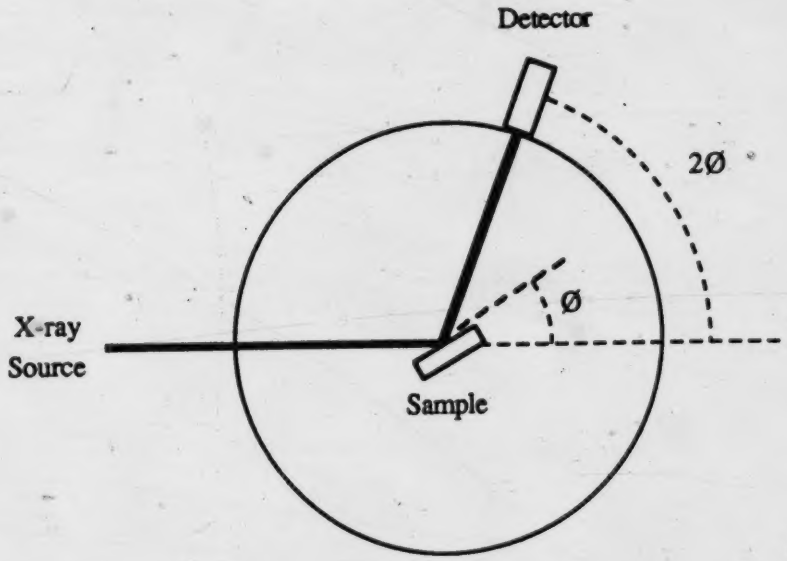

Figure 4.4 A schematic diagram of a X-ray diffractometer.

The calculated interplanar spacings were compared to the interplanar spacings of the compounds thought to exist in the films (InN, In_2O_3, and In) and from this, the crystallite phases in the film were determined. The interplanar spacings of these compounds were found in the ASTM X-ray powder files. These files are a tabulation of crystallographic information on many different materials and are central to the identification of crystalline phases in materials [51]. Comparing the interplanar spacings of InN, In_2O_3, and In, to the interplanar spacings observed in the XRD spectrum (Figure 4.3), found that all the peaks, except one, could be identified as InN (see Table 4.1).

The unassigned peak, at 38.22°, is due either to InN (101) or to In_2O_3 (110) planes. This peak is tentatively identified as InN (101), because a number of InN thin films grown by other workers have been strongly (101) oriented [2,23,25], although the possibility of the peak being due to In_2O_3 cannot be discounted.

Angle 2θ	Interplanar Spacing (Å)	Powder Interplanar Spacing (Å)	Peak Assignment	Shift
36.31°	2.871	2.85	(002) InN	+0.7 %
38.22°	2.732	2.70	(101) InN	-1.0 %
			or	
		2.747	(110) In_2O_3	+0.6 %
50.30°	2.105	2.090	(102) InN	+0.8 %
66.78°	1.625	1.614	(103) InN	+0.7 %

Table 4.1 Identification of XRD peaks for the film deposited at 90 W.

From this analysis of the XRD spectra, the films were found to consist of a number of different crystallites of the basic InN hexagonal wurtzite structure. The strength of the (002) diffraction peak suggests that the films were mainly made up of hexagonal wurtzite crystallites oriented with their c axes perpendicular to the substrate surface. This type of structure for InN has been reported by a number of different authors [6,24] and seems to be the preferred orientation of growth for materials, such as AlN [9] and ZnO [52], that have the hexagonal wurtzite structure.

Homogeneous strain in the thin film either expands or contracts the interplanar spacing of the diffracting plane [50]. This stress is measured by comparing the interplanar found in the powder files, which are for unstressed powders, with the

measured interplanar spacing. Using this comparison it is found that the lattice of the InN has expanded by 0.7%. Stress of this magnitude is typical for reactively sputtered thin films [52].

The diffraction peak is broadened by a number of effects: inhomogeneous stress in the film, instrumental effects, and the finite size of the crystallites [50,51]. If the broadening due to the instrumental effects and inhomogeneous strain can be accounted for, the size of the crystallites can be found using Scherrer's equation:

$$t \leq \frac{0.95\,\lambda}{B\cos(\theta_b)} \qquad (4.2)$$

where t is the size of the crystallites, λ is the wavelength of the x-rays, θ_b is the Bragg angle of the diffraction peak and B is the full width of the peak at half the maximum intensity (FWHM line width) due to the crystallite size. If the effects due to the instrumental and inhomogeneous stress broadening are neglected the minimum size of the crystallites can be calculated using the above equation. The minimum crystallite size for (002) oriented crystals was found to be 20 nm, which is also typical for reactively sputtered thin films [52].

In summary, the general features of the XRD spectra of these sputtered InN thin films contain no surprises. The InN films are polycrystalline and the deposited material is identified as InN not indium oxide or some intermediate phase, although there is a possibility of a crystalline indium oxide phase being present. The homogeneous stress in the film and the minimum crystallite size are typical for reactively sputtered thin films [52] and for InN deposited by other workers [26,53].

The crystalline structure and the columnar structure of the thin film are determined by XRD and SEM cross sections respectively. The crystal structure and the columnar

growth structure are related but the actual relationship between these two types of structures is presently unknown [45]. The root of this problem is that the structure zone models, as they now stand, are only qualitative in nature. At present, the crystal structure and the columnar structure of the films must be treated separately, as they have been here.

4.2 Bandgap Determination

For many semiconductor thin films the measurement of the absorption near the bandgap energy is the most commonly measured optical property, since many effects manifest themselves in changes in the absorption in this region [54]. In particular, the value of the bandgap can change dramatically with the composition and structure of the film [55,56]. These different values of the bandgap should be labelled as the 'effective' bandgap, because they are due to changes in the allowed states near the bandgap, and not due to changes in the material [54]. Unfortunately, experimentally measured values of the effective bandgap are often incorrectly reported in the literature as simply the material's bandgap. However, for relatively unstudied materials such as InN where the bandgap has not been firmly established, all values of the bandgap must be assumed to be valid values of intrinsic bandgap, until such time as the literature agrees on a particular value.

The bandgap of a semiconductor is determined from the onset of absorption in the transition region between the transparent and the conduction band absorption regions of the optical spectra. The absorption coefficient for a direct bandgap semiconductor near the band edge is expected to follow [57]:

$$\alpha = A\,(E-E_g)^{1/2} \qquad (4.3)$$

where α is the absorption coefficient, E is the incident light energy, E_g is the energy of the bandgap, and A is a constant. The bandgap can be determined by plotting the square

of the absorption coefficient versus the incident energy. As shown in Figure 4.5, such a plot consists of a linear section, which corresponds to equation 4.3, and a tailing of the absorption at lower energies. By extrapolating the linear portion of the curve to zero absorption the bandgap energy can be determined.

Films grown on quartz substrates, which are transparent in the region of interest (1.0 to 3.0 eV), were used in determining the bandgap of the InN films. The transmission and reflection spectra were measured using a Cary 2400 UV-NIR spectrophotometer and the dual beam reflectance accessory. To precisely determine the absorption coefficient in the bandgap region, one should use the equations for determining the optical constants in the strongly absorbing region as given in Chapter 6. However, for convenience most authors use an approximation:

$$\frac{T}{1-R} = e^{-\alpha d} \qquad (4.4)$$

where T is the transmission, R is the reflection, d is the thickness of the film, and α is the absorption coefficient. This approximation assumes that all of the reflected light comes from the first interface (air/film), and yields the absorption coefficient to within 5 %.

The plot of the square of the absorption (Figure 4.5) shows that the sputtered InN thin film has a bandgap of 1.7 ±0.05 eV. The measurements reported in the literature have placed the bandgap of InN between 1.7 and 2.1 eV [1], placing our values at the low end of this range. A bandgap of 1.7 eV further supports the XRD data in identifing the material as indium nitride and not In_2O_3 (E_g=3.2 eV) or an indium oxynitride, since the films show no evidence of a band edge due to the presence of a crystalline In_2O_3 phase.

The value of the bandgap determined from the low carrier concentration films of Tansley and Foley (1.89 eV) [1] is most likely the intrinsic value of the bandgap for InN,

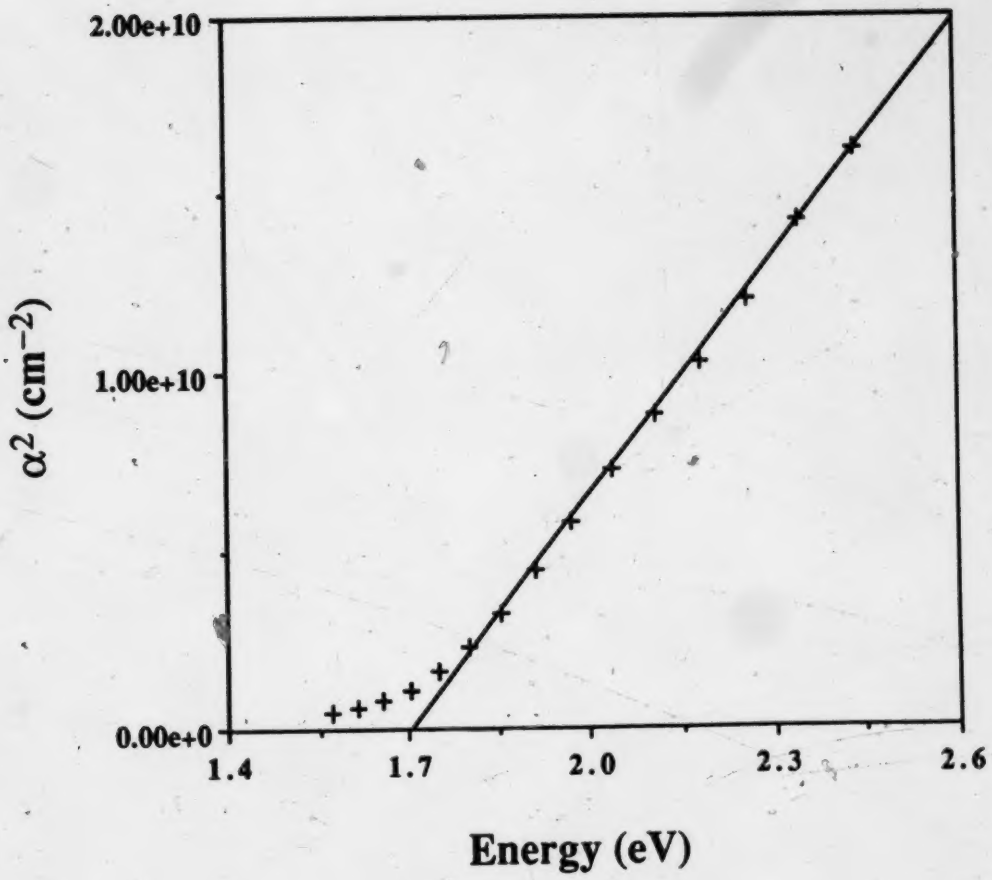

Figure 4.5 The square of the absorption coefficient near the band edge and the linear extrapolation used to determine the bandgap.

with most of the other differing values caused by bandgap widening and narrowing effects. These effects, which increase or decrease the effective size of the bandgap, are due to two different, but related effects. In degenerate semiconductors, the electrons (for an n type material) fill the bottom states in the conduction band, causing the onset of absorption to be shifted to higher energies, and effectively increasing the width of the bandgap [54,55,56,58]. This effect, called the Burnstein-Moss effect, has been seen in many degenerate semiconductors and is very common in semiconductor thin films. The effective size of the bandgap can also decrease due to the extending of the valance and conduction bands into the bandgap due to electron-electron and electron-ion scattering effects [54,56]. The bandgap widening and narrowing effects occur simultaneously in most semiconductors and the effective bandgap depends on which effect dominates.

In imperfect semiconductors, the absorption near the band edge is larger than expected from equation 4.3. Such excess absorption was originally identified by Urbach [59] and is found to decrease exponentially with energy. The actual cause of the Urbach absorption tail is presently unknown, although the generally accepted explanation is that it is due to localized perturbations in the position of the bottom of the conduction band and the top of the valence band caused by defects and impurities in the material [5]. From Figure 4.6, the absorption below the band edge in this InN film is found to contain an Urbach absorption tail, since the absorption curve is exponential.

A majority of the bandgaps reported in the literature are larger than the intrinsic bandgap measured by Tansley and Foley (1.89 eV). Tansley and Foley have developed a empirical relation that relates bandgap values to carrier concentrations [1]. This empirical expression ($E_g=1.89+2.1\times10^{-8}\ n_e^{1/3}$) has a different exponent than predicted by Burnstein-Moss ($n^{2/3}$). This led Tansley and Foley to propose that significant band narrowing also occurs in InN. It is possible that the electron-electron and electron-ion

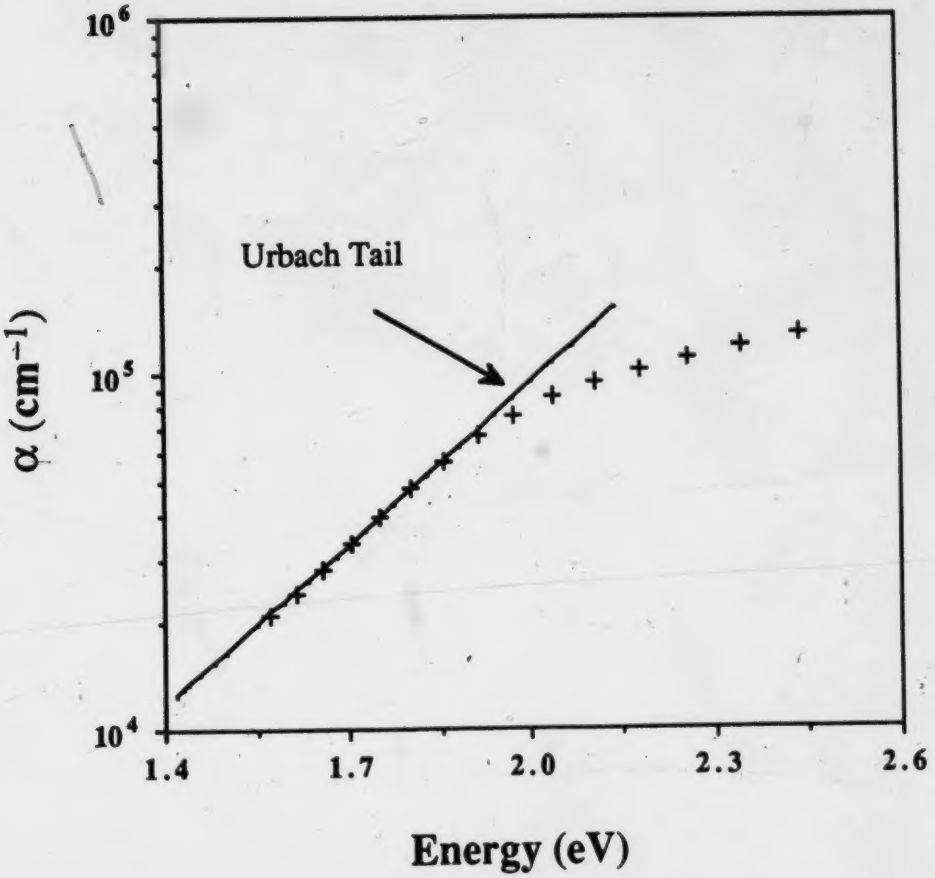

Figure 4.6 The absorption near the band edge shows the presence of an Urbach absorption tail.

interactions responsible for the bandgap narrowing could also be related to the low electron mobilities that are seen by most other researchers.

This work and that of a few others [25,27], have reported bandgaps with energies less than the bandgap measured by Tansley and Foley (1.89 eV). From a replotting of the absorption data of Hovel and Cuomo, Tansley and Foley have proposed that films with bandgaps less than 1.89 eV contain defect states that are responsible for the narrower bandgap. The replotted data of Hovel and Cuomo shows a linear region at higher energies that extrapolates to the bandgap value predicted by Tansley and Foley's empirical formula and a second linear region at lower energies that extrapolates to 1.7 eV. However, this second higher energy transition is not evident in our bandgap absorption measurements (Figure 4.5). The cause of the lower bandgap value in our samples is not known.

In summary, the bandgap of the InN films, deposited at 90 W, was measured and found to be 1.7 eV. The absorption data show excess absorption at lower energies that can be explained by the presence of an Urbach absorption tail. The bandgap is smaller than for most films reported in the literature and, more importantly, smaller than the intrinsic value of 1.89 eV as determined by Tansley and Foley. The cause of this lower bandgap energy is unknown, but it could be caused by the electron-electron and electron-ion interactions or it could be caused by defect states.

4.3 Resistivity and Film Thickness

The thicknesses of the deposited films were measured using a mechanical surface profilometer (Tencor Alpha-Step model 100) over a step on the 7059 glass formed by a shadow mask (microscope cover slip). The uncertainty in the thickness measurement is ±10%, because of non-uniform thickness of the film and the difficulty in producing a sharp edge using a shadow mask. The films deposited in this study were between 0.1

and 1.0 μm thick. The deposition rate of the InN thin films was approximately 5 Å/s which is also typical for sputtered film deposition, although a little low.

The resistivity of the InN thin films was determined from the thickness of the film and from a four point probe measurement of the sheet resistance of the film resistance. In this calculation of the sheet resistance, the geometric factor for a semi-infinite film on a insulating substrate ($\pi/\ln 2$) [60] was used. The use of this factor is valid because of the large size of the sample (25 mm) compared to the probe tip spacing (1 mm) and because the films are significantly thinner than the probe tip spacing. The resistivity (2.5×10^{-3} Ω-cm) is similar to those reported by other authors. The error in the resisitivity is ±10 %, mainly due to the error in the film thickness. A Veeco model 1200 four point probe was used in these measurements. Both the four point probe and the surface profilometer are located in the fabrication facility at the Alberta Microelectronic Centre.

4.4 Hall Probe Analysis

The carrier concentration and the carrier mobility of the thin films were measured using a standard Hall probe technique [61]. The Hall probe pattern was formed using a shadow mask on a Corning 7059 glass substrate. The connections between the instrumentation and the thin film were made using wires bonded to the InN thin film using 'silver paint' (silver particles suspended in a solvent).

The electrical properties of the thin film are related to the voltage that is induced across the Hall probe sample by the magnetic field, by the Hall probe equation [61]:

$$R_h = \frac{V d}{B I} \qquad (4.5)$$

where R_h is the Hall coefficient, V is the voltage that is induced across the sample (Hall voltage), B is the applied magnetic field, I is the current, and d is the film thickness.

The type of majority carriers (electrons or holes) is determined from the sign of the Hall coefficient. The carrier concentration is determined from $n_e=1/(R_h q)$, where q is the charge of an electron. The majority carrier mobility of the film is determined using $\mu_h=R_h/\rho$ where ρ is the resistivity of the film. The mobility measured using the Hall effect (μ_h) is related to the actual carrier mobility (μ) by $\mu_h=r_h\mu$, where r_h is a factor that is related to the dominant type of carrier scattering in the film. Depending on the dominant scattering centre, r_h can have a value between 1 and 2. For degenerate semiconductors, such as InN films, r_h is assumed to be 1 [61].

An electromagnet with a field swing of 1.2 Tesla was used in these measurements to provide the magnetic field perpendicular to the film surface. A constant current of between 0.5 mA to 10 mA was used, depending on the film thickness. The Hall voltage, across the sample, was measured using a HP model 3468 B digital voltmeter and was typically about 30 μV. The Hall probe equipment was tested using a ZnO Hall probe pattern that had been characterized at the University of British Columbia.

The Hall probe measurements of the InN thin films determined that the majority carriers are electrons (n type material); this is consistent with the InN films reported in the literature. The carrier concentration is typically $3x10^{20}$ cm^{-3} ±10 % and the electron mobility is 7.0 cm^2/Vs ±5 %. The electron mobility of these films is within the range reported, in the literature, by a majority of the workers (2 to 50 cm^2/Vs) [21,22,23,24,25]. The carrier concentration is also consistent with those reported elsewhere for these low mobility films. The low electron mobility found in these experiments indicates that there are many scattering centres throughout the bulk film and that high electron mobility InN thin films could be difficult to obtain.

4.5 Rutherford Backscattering

The bulk film stoichiometry was determined for a number of samples using Rutherford backscattering spectroscopy (RBS). RBS is a useful stoichiometric characterization tool because of its sensitivity to low atomic mass elements and it does not require standards [62]. However, it does not provide any information on how the elements are bonded and the area in which the measurements are taken is quite large (1 mm^2). The RBS measurements were performed at McMaster University approximately three weeks after the films were deposited. These measurements, as well as an earlier set analyzed at the University of Salford, UK, represent the first measurement of the bulk stoichiometry of InN thin films.

In RBS, the stoichiometry is determined from the ratio of the number of atoms of element a to element b. This ratio is given by [62]:

$$\frac{N_a}{N_b} = \frac{A_a \, \sigma_b(E_0)}{A_b \, \sigma_a(E_0)} \qquad (4.6)$$

where: N_a and N_b are the number of atoms of element a and b repectively, A_a and A_b are the areas under the curves corresponding to the elements a and b, and σ is the Rutherford scattering cross section for an incident helium beam energy (E_0) and is tabulated in reference 62. The area that corresponds to each element (see Figure 4.7) is found by removing both the background and the contribution caused by the overlap of the curves of other elements [62]. The error in the RBS measurement is in large part caused by the error in the measurement of the area under the curves. The error in this analysis is $\pm$ 0.04 for the N/In ratio and $\pm$ 0.02 for the O/In ratio. Table 4.2 shows the measured stoichiometries of two InN films deposited at different deposition powers.

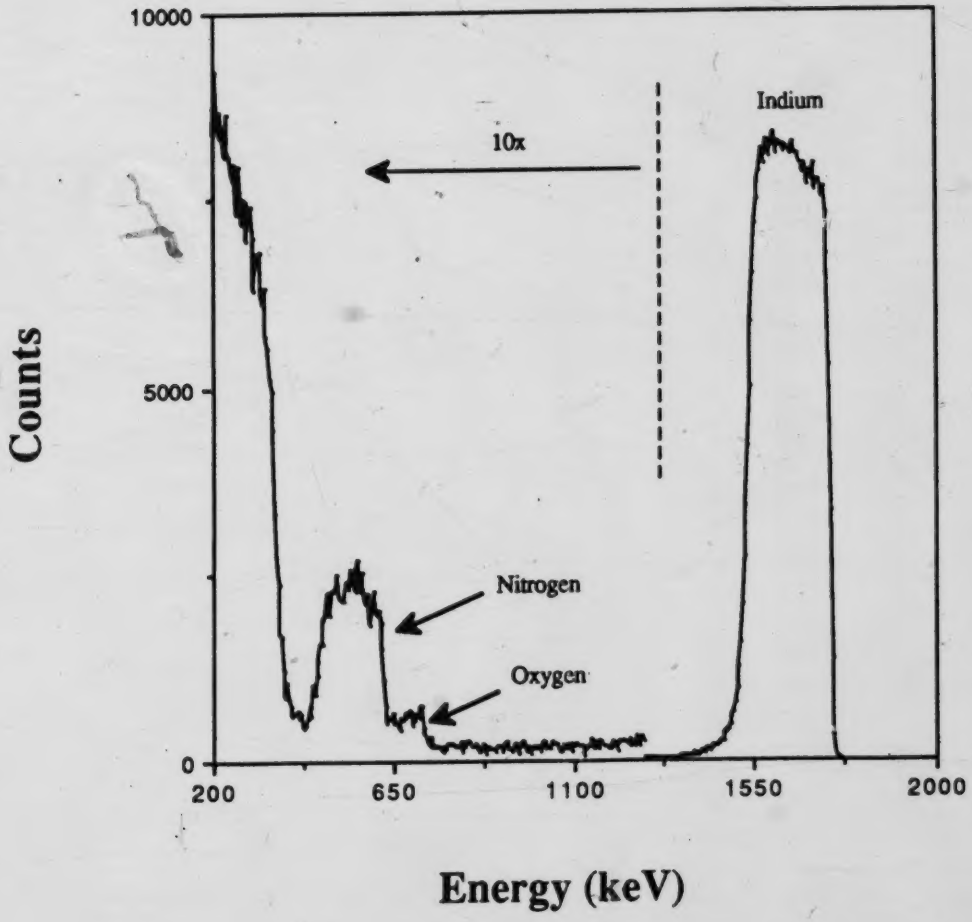

Figure 4.7 RBS spectrum for the film deposited at 90 W. The incident ^{4}He energy was 2.0 MeV.

Deposition Power	N/In	O/In	Formula
90 W	0.98 ±0.04	0.24 ±0.02	$In_{0.45}N_{0.44}O_{0.11}$
150 W	1.01	0.203	$In_{0.45}N_{0.45}O_{0.10}$

Table 4.2 The bulk stoichiometry of InN thin films as determined by RBS. The base pressure was $1x10^{-7}$ torr prior to deposition.

This bulk stoichiometry study yielded two surprising results. First, a large amount of oxygen (10 at. %) was found throughout the film thickness and second, even with the large amount of oxygen present in this film, the indium to nitrogen ratio was still 1:1.

Since this RBS measurement is the first reported study of the bulk stoichiometry of InN thin films, it is very likely that other InN films reported in the literature also contained significant amounts of oxygen. This is because the XRD, bandgap, and electrical properties of the InN films characterized here are very similar to those films. Also, most of the films reported in the literature were deposited at higher base pressures ($> 10^{-6}$ torr) than those used to deposit our films.

4.6 Summary of the characterization of the InN thin films

Thin films of InN were deposited by DC planar magnetron sputtering in pure nitrogen discharges at base pressures in the low 10^{-7} torr range. These films were characterized using SEM cross sections, XRD, optical bandgap measurements, and electrical measurements. Bulk composition was determined using Rutherford backscattering analysis.

The structural characterization by SEM cross section and XRD shows the films to have a columnar microstructure and to have a crystal structure made up of crystallites of

hexagonal wurtzite InN, and not In_2O_3 or any intermediate indium oxy-nitride phases. The bandgap was found to be 1.7 eV, which is indicative of InN. There was no clear evidence of an absorption edge due to In_2O_3. Thus the XRD and bandgap measurements suggest that the crystal structure of the films is made up of InN grains, with no In_2O_3 phases being present.

The low electron mobility and high carrier concentrations suggest that the films are highly defected with many scattering centres throughout the film. The RBS analysis supports this suggestion since it shows the films have more oxygen and nitrogen than can bind stoichiometrically to the indium. The precise bonding arrangement between the indium, oxygen, and nitrogen is unknown, but from the XRD and bandgap analysis, we conclude that the oxygen is probably not bound in a crystalline form.

Chapter 5

Discussion of the Results

The characterization of the InN films in the previous chapter and in the appendix has presented a number of perplexing results. The stoichiometry study of the film bulk shows the presence of significant oxygen contamination but the ratio of indium to nitrogen in the films is still 1:1. Also, the XRD and optical bandgap analyses show no clear evidence of the oxygen contamination or significant amounts of stress in the films due to possible interstitial nitrogen and oxygen atoms. Finally, the electron mobilities of the films were low (6 to 10 cm^2/Vs) and the carrier concentrations were large ($3x10^{20}$ cm^{-3}) and these electrical properties appear to be insensitive to changes in the deposition conditions.

5.1 Stoichiometry of Nitrides

To better understand the stoichiometry and XRD data of the InN films, a search was made of the literature of sputtered metal nitrides. Recently, the stoichiometry of refractory nitrides has been studied in some detail by a number of authors, because of their potential applications as barrier layers in microelectronics and hardness coatings. This research has shown that the oxygen contamination, excess nitrogen and the lack of evidence of oxide or oxy-nitride phases found in the InN films are common to other nitrides. In particular, nitrides of Ti [63,64,65,66,67], Zr [63,67], Ta [68], and Hf [67] were deposited by planar magnetron sputtering. The bulk stoichiometry of these films showed the presence of 1 to 15 % at. oxygen and a nitrogen to metal ratio which varies between 0.99 to 1.35, even though these films were deposited at base pressures less than 10^{-6} torr. Only the presence of mono-nitride phases was detected in the XRD and TEM studies and there was no evidence of oxides or oxy-nitrides.

5.2 Oxygen Contamination

The large amounts of oxygen found throughout the bulk of these films, both for InN and other nitrides, is surprising considering the low base pressures in the sputter chambers. The maximum amount of oxygen contamination of the InN films due to incorporation during sputtering by the residual gases was calculated and found to be 0.3 at. % due to O_2 and 3.0 at. % for water vapour. The actual contamination due to water vapour is felt to be much lower than this because of the non-spontaneous reaction between water vapour and indium, found using the heats of formation calculations. The oxygen contamination of the films during sputtering by the residual gases is insufficient to account for the amount of oxygen seen throughout the film bulk by the RBS analysis (10 at. %).

A similar phenomenon has been reported by Williams et al. [66] for reactively sputtered TiN at base pressures below $1x10^{-6}$ torr. The stoichiometry of the films was measured and the nitrogen to titanium ratio and the oxygen to titanium ratio were found to be 1.11 and 0.25 respectively. XRD and TEM studies of the films showed evidence of TiN phases, but not of oxynitride phases or of higher nitrides. To understand the stoichiometry results they calculated the maximum amount of oxygen contamination caused by the residual gases in the sputter chamber. Williams et al. came to the same conclusions as I do for InN, namely, that the residual gas pressures during sputtering could not account for the amount of oxygen measured in the stoichiometry study. To account for the extra oxygen, they proposed that the majority of the oxygen seen in the stoichiometry study was due to surface oxidation, which occurs after the film is removed from the sputter system and exposed to air. The oxygen was seen throughout the film bulk because not only did the surface of the film oxidized, but the surface of the columnar growth structure also oxidizes. Since the columnar structure extended through the whole

film bulk this surface oxidation was seen throughout the film bulk. This surface oxidation was most likely amorphous, since it is not seen in the XRD or TEM studies.

Oxidation of the column surfaces could occur in InN films since there exists evidence for surface oxidation of InN. A number of surface stoichiometry studies have reported the presence of oxygen on the surface of InN [69,70,71]. The InN surface oxidation study of Foley and Lyngdal [69] has shown that oxygen is bound in an N-O complex and not as In_2O_3. In this work, the RBS study shows an increase in the oxygen content of the films near the film surface, which is indicative of surface oxidation. Moreover, the heat of formation analysis also suggests reactions between O_2 and InN are possible. Furthermore, the spectroscopic ellipsometry study of InN shows evidence of oxidation of InN after deposition [28]. The optical constants of InN, from 2.5 to 5.5 eV, were measured immediately after deposition and after the samples were exposed to air for a number of days. The optical constants of the films changed after exposure to air with a good fit being achieved by assuming that the films took up 4 volume % of In_2O_3 while exposed to the air. Thus there is a significant body of research that strongly suggests that the surface of InN does oxidize.

From the work of Williams et al. and the evidence of surface oxidation of InN, it is proposed that almost all of the oxygen seen in the RBS stoichiometry study of the InN thin films results from the oxidation of the column boundaries after the samples were removed from the sputter system. This surface oxidation is probably amorphous and this is why there is no evidence of crystalline indium oxide or oxy-nitride phases. However, this does not explain the low electron mobilities of these InN samples since the electrical data suggests that the scattering centres in the InN films are present throughout the film bulk rather than only on the surfaces of the columns.

5.3 Low Electron Mobility

The calculation of mean free path of the electrons in these InN films (see Chapter 6) suggests that scattering centres exist throughout the bulk of the films. The calculated mean free path of the electrons between collisions is approximately 2 nm, which is significantly smaller than the minimum size of the crystallite as found by XRD (20 nm). This implies that the scattering centres are incorporated into the films during growth and are not incorporated after deposition by the oxidation of the InN column surface.

Various authors have suggested that the low electron mobility of the InN films is due to the presence of nitrogen vacancies in the films [7,33,21], which are caused by the low reactivity of indium with nitrogen. Another possible source of scattering centres could be the small amount of oxygen that is incorporated into the film during sputtering. A number of groups have studied the effects of oxygen impurities in AlN and GaP [72,73]. They found that oxygen in these materials acts as a deep electron donor state. It was also found that the solid solubility of oxygen in AlN is large ($5x10^{21}$ cm^{-3}) [72] and that if all of these oxygen atoms were to act as deep donor states, the carrier concentration in AlN would be very large. If oxygen were to act the same way in InN, then the 0.3 at % oxygen which can be incorporated into the InN films during deposition would be sufficient to account for the carrier concentrations which are actually seen in these films. There is some evidence that this does occur in the InN thin films.

By plotting all reported electron mobilities versus their carrier concentrations for InN (Figure 5.1) it becomes apparent that a relationship exists between the source of the electrons and the scattering centres in the films. This plot shows that a decrease in the electron concentration corresponds to an increase in the electron mobility and vice versa. This direct relationship implies that the source of the electrons and the scattering centre are the same: an ionized impurity. This is further supported by the optical absorption

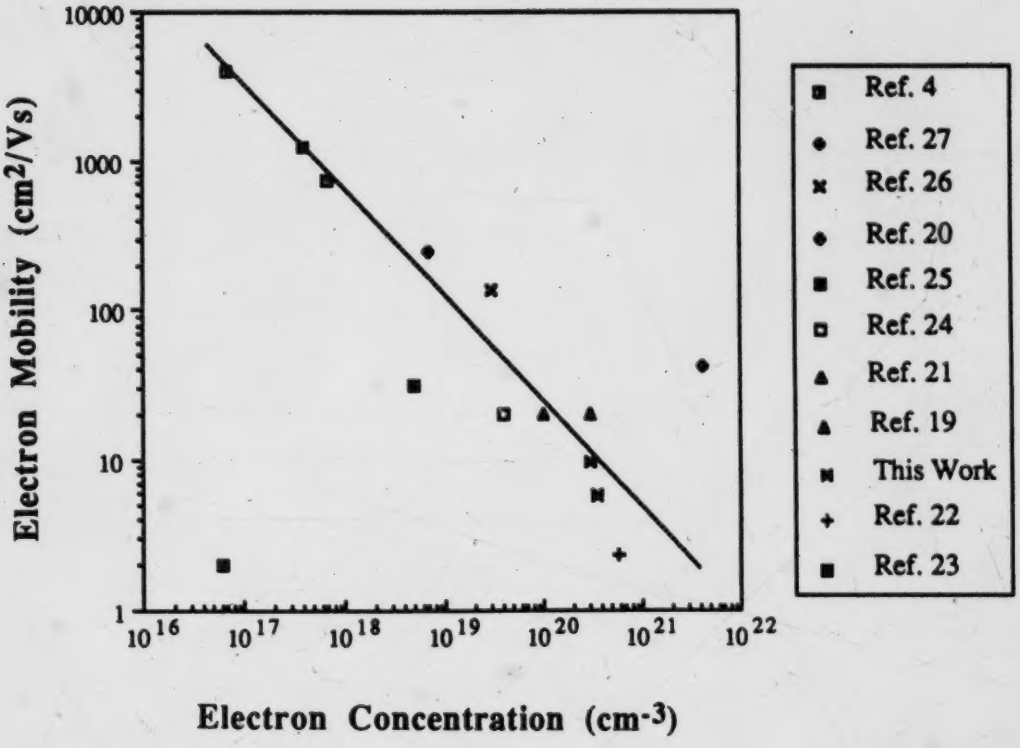

Figure 5.1 The electron mobilities and concentrations of InN films reported in the literature.

measurements in Chapter 6, which identify the dominant scattering centre in these films as an ionized impurity. This evidence, along with the data from AlN suggests that the cause of the low mobilities in the InN films is an ionized oxygen impurity.

The incorporation of the ionized oxygen impurity into the lattice of InN is possibly enhanced by the low reactivity of indium and nitrogen. It is conceivable that the nitrogen vacancies or unsatisfied indium bonds in the InN lattice are filled by oxygen atoms during deposition. However, if there are few nitrogen vacancies then very little oxygen can be incorporated into the crystallites. Reducing the oxygen content of the crystallites would decrease the number of scattering centres and thus, it would increase the electron mobility of the film. This increase of the electron mobility by decreasing the number of nitrogen vacancies could explain why Tansley and Foley [3,4] succeeded in depositing InN with high electron mobility, when everyone else failed. If one carefully reviews the techniques they used to deposit their films, a number of the ways they reduced the nitrogen vancancy concentration in their films are identified. The main method being the very low deposition rates used (315 hours) [6]. At these low deposition rates, there was a long time for the indium bond to be satisfied by a nitrogen atom before the indium bond is buried beneath the next layer of indium or filled by an oxygen atom. The indium bond would not be immediately filled by oxygen atoms, as would happen in most sputter systems, because the residual oxygen pressure in their sputter chamber was very low. The residual oxygen pressure in their sputter system was low because the sputter chamber they used was quite small, and was baked at high temperatures [74] prior to the deposition of their films. More significantly, any oxygen in the system would be getter pumped by the first few layers of InN that were deposited during the initial portion of the deposition. The excessively long sputter times used by Tansley and Foley are not useful for depositing films, although the procedure of saturating all the indium bonds with nitrogen could be useful for depositing high electron mobility InN films.

5.4 Summary

The oxygen contamination and the excess nitrogen which were seen in the InN films characterized in chapter 4, appears to be typical for sputtered nitrides. From the calculation of the maximum oxygen content due to residual oxygen, it is proposed that a almost all of the oxygen in the films is incorporated by oxidation of the surfaces of the columnar structure of the films. The oxygen is possibly bound in an N-O complex, as suggested by Foley and Lyngdal [69], which could explain why the oxygen is not seen in the XRD or the optical absorption measurements.

The optical absorption study reported in chapter 6 identifies the scattering centre in my InN films is an ionized impurity. Further evidence from the literature of InN and other wide bandgap semiconductors supports the contention that the ionized impurity reponsible for the low electron mobilities of my InN films is oxygen that is incorporated into the film during sputtering. By reducing number of nitrogen vacancies in which this oxygen can be incoporated into the film, the electron mobility of the films should increase.

Chapter 6

Optical Constants of InN

The lack of study of InN is exemplified by the dearth of information on its optical constants. Apart from measurements of the absorption near the band edge, the optical properties of InN have been reported in only certain spectral regions and with little detail. The only systematic study of the optical properties of InN was performed by Tyagai et al. [19] who measured the optical constants, n and k, in the important region below the band edge (500 to 3000 nm). They also measured and modelled the infrared reflectivity in the near infrared region (2 to 4 μm) using the Drude theory of free electrons. This modelling of the reflectivity provides the only experimental determination of the electron effective mass, a constant which is extremely important in understanding the high electron mobilities reported by Tansley and Foley [3,4]. The only other measurements of the index of refraction in the 1 to 2 μm region have been for selected wavelengths by a few authors [25,27]. In the infrared, the transmission spectrum of InN in the region of 0.6 to 30 μm has been measured [75]. Also in the infrared, the phonon absorption bands (Restrahlen bands) of InN have been measured by extrapolating from the Restrahlen bands of GaInN alloys [15].

Until recently, the optical constants above the band edge (500 nm) could only be inferred from a single measurement of the reflectivity of InN in the 200-400 nm range [53]. However, as part of this research, the optical constants in this range were determined using spectroscopic ellipsometry [28]. The films were grown and partially characterized here at the U of A, while the optical measurements and analysis were performed by Dr. B. Sullivan at the University of British Columbia.

This chapter reports the measurement of the optical constants from 700 to 2700 nm, for two films, one deposited at 90 W and the other at 150 W. The transmission and reflection spectra of the films were measured using a spectrophotometer and the optical constants were determined using two different analysis techniques. From these optical constants the dielectric constant of the lattice was determined, as well as the dominant scattering mechanism. The infrared reflectivity in the range 2.5 to 20 μm was measured for the two films and the optical properties of the films were modelled in this region using the Drude theory of free electrons. The optical effective mass of the electron in InN was determined by fitting the calculated reflectivity to the measured reflectivity.

6.1 Measurement of the Optical Constants

The transmission spectrum of a typical semiconductor consists of three different regions [57]. The first region is a region of high absorption above the bandgap. The optical constants in this region are dominated by interband transitions and by the structure of the conduction band. The second region lies in the infrared portion of the spectra. The optical constants in this region are related to both the phonon structure of the material and effects caused by free carriers. The third region, the forbidden bandgap region, lies between these other two regions and is characterized, in ideal semiconductors, by no absorption. However, in real semiconductors, there exists some absorption from impurity states in the bandgap, tailing of the free electron absorption into this region from the infrared [57], and from the presence of an Urbach tail near the band edge [59]. In the transparent region it is possible to determine the optical constants fairly easily using spectrophotometric techniques [76,77]. For thin films deposited on transparent substrates, the transmission spectrum of the transparent region of the film is dominated by an interference structure caused by constructive and destructive interference of the incident light . This structure can be seen in the transmission spectrum of the InN film deposited at 90 W, shown in Figure 6.1.

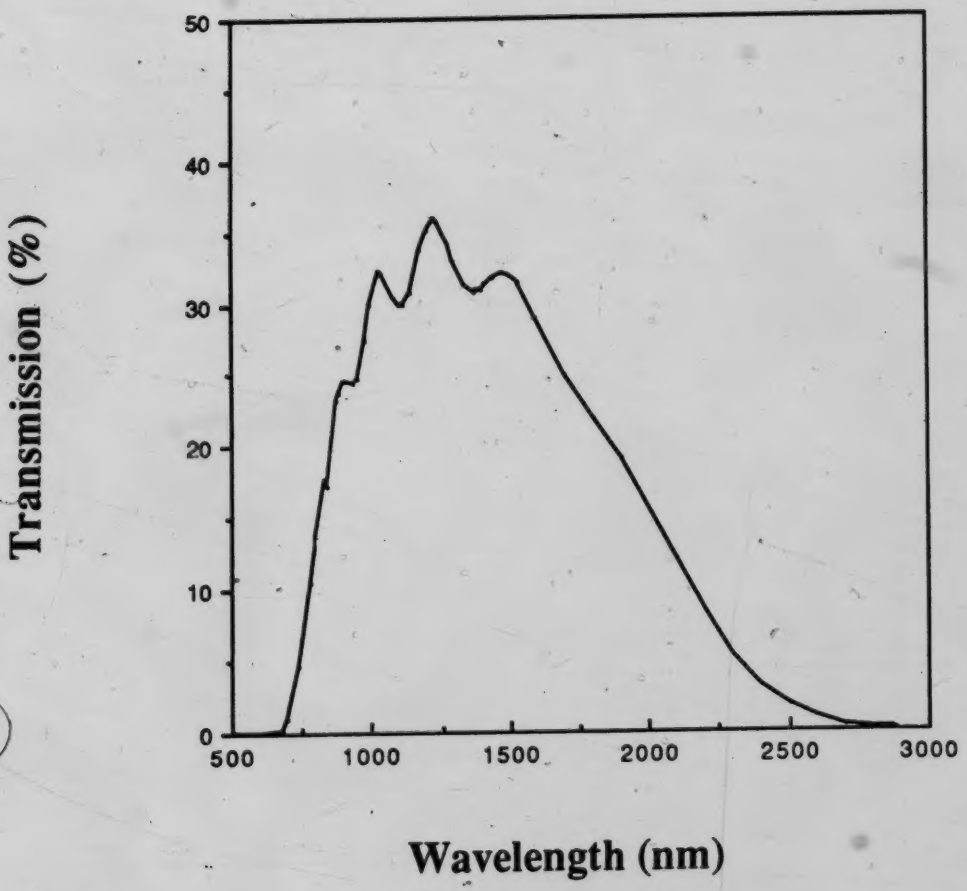

Figure 6.1 Transmission spectrum of InN film deposited at 90 W.

The optical constants in the transparent region of the InN thin films were calculated using two techniques, one in the weakly absorbing region and one in the strongly absorbing region. In the strongly absorbing region, an iterative technique, based on standard equations for the transmission and reflection from a film/air stack was used to calculate the optical constants [77]. In the weakly absorbing region the optical constants were measured using only the transmission spectra and the technique developed by Swanepoel [76]. In the regions where these two techniques overlap, the results were compared and verified.

Experimentally, the transmission and reflection spectra of the InN thin films deposited onto quartz substrates were measured using a Cary 2400 UV-NIR spectrophotometer and the dual beam reflectance accessory. The thickness of the film was determined using the surface profilometer. The films grown on quartz were used in this study because the optical constants of quartz in this region are well documented [78,79] and it is transparent from 200 to 3000 nm.

6.1.1 Weakly Absorbing Region.

In the weakly absorbing region, the optical constants were calculated with a technique developed by Swanepoel [76], which uses the interference structure of the transmission spectra. The advantage of this technique is that only the transmission spectra is required rather than both the transmission and reflection spectra, to calculate the optical constants. This is advantageous because reflection measurements are prone to error and reflectance accessories for spectrophotometers are uncommon.

The technique of Swanepoel is an extension of an earlier technique developed by Manifacier et al. [80]. Swanepoel extended the technique to take into account the reflection from the substrate/air interface at the back of the film/substrate stack. Swanepoel's technique is derived from the equations for the transmission of light through

a film/substrate stack and from the equations for the constructive and destructive interference. The derivation is involved, but the results are straight forward. The final equations relate the optical constants of the film to an envelope defined by the extrema in the transmission spectrum. The envelope consists of two curves, one that connects the interference maxima and the other the minima (Figure 6.2). The optical constants and the thickness of the film are related to this envelope by:

$$n=[N+(N^2-s^2)^{1/2}]^{1/2} \tag{6.1}$$

$$e^{-4\pi kd/\lambda}=\frac{\left[G-\left\{G^2-(n^2-1)^6(n^2-s^4)^2\right\}^{1/2}\right]^{1/2}}{(n-1)^3(n-s^2)} \tag{6.2}$$

where:

$$N=\frac{s^2+1}{2}+2s\frac{T_{max}-T_{min}}{T_{max}T_{min}} \tag{6.3}$$

$$s=\frac{1}{T_s}+\left(\frac{1}{T_s^2}-1\right)^{1/2} \tag{6.4}$$

$$T_s=\frac{(1-R)^2}{1-R^2} \tag{6.5}$$

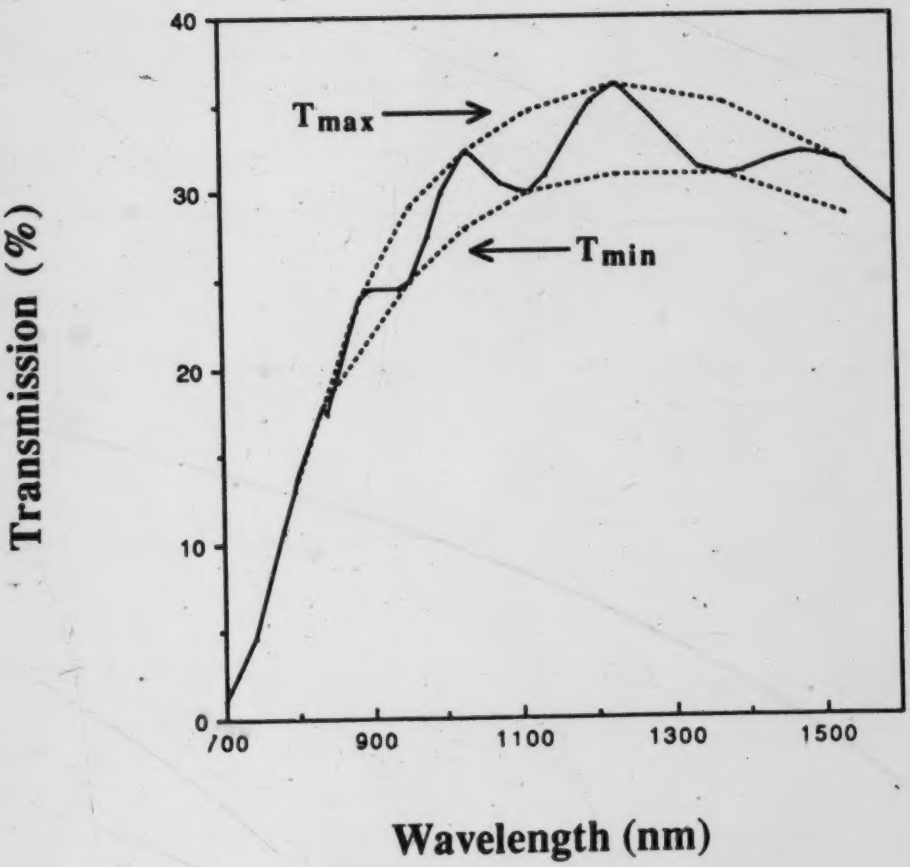

Figure 6.2 Transmission spectrum of the film deposited at 90 W in the weakly absorbing region. The curves that connect the interference extrema are shown.

and

$$G=\frac{128n^4s^2}{T_{max}T_{min}}+n^2(n^2-1)^2(s^2-1)^2+(n^2-1)^2(n^2-s^2)^2 \qquad (6.6)$$

where R is the reflection from an air/substrate interface, n and k are the optical constants of the film, and T_{max} and T_{min} are the values of the envelope. The thickness of the film is found using the observation that the order of the interference extrema must be exactly a full or half integer.

The optical constants and the film thickness of two InN samples were determined using these equations. The optical constants of the film deposited at 90 W are shown in Figure 6.3 and 6.4. The film thicknesses as determined by this technique were 1.1 μm and 1.0 μm for the 90 and 150 W films, respectively. This compares favorably with the thicknesses determined using the surface profilometer (1.0 μm and 1.0 μm). The error in the optical constants calculated using Swanepoel's technique was found to be +/- 5 % for n and +/- 15 % for k.

6.1.2 Strongly Absorbing Region

To calculate the optical constants in the region of strong absorption, an iterative technique was used. This technique is based on calculations of the reflected and transmitted spectra, using standard equations for the transmission of light through a film/substrate structure [77]. For the two InN films that were studied, there are two regions where the strongly absorbing approximation can be used to calculate the optical constants: 700 to 900 nm and 1500 to 2700 nm.

The total transmission and reflection of light through a film/substrate structure can be written as arithmetic series which takes the reflection from the various interfaces (Figure

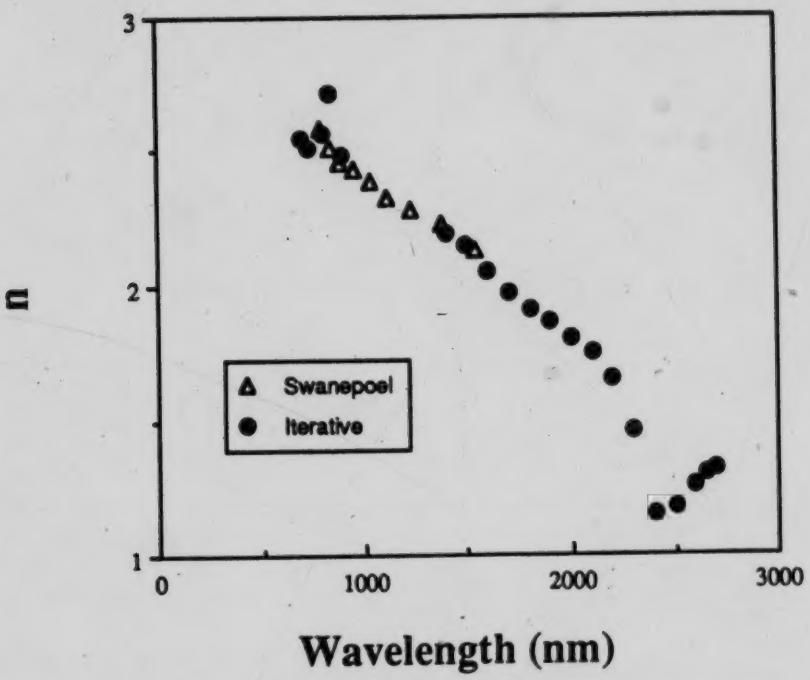

Figure 6.3 The index of refraction (n) of the film deposited at 90 W film calculated using the two different techniques.

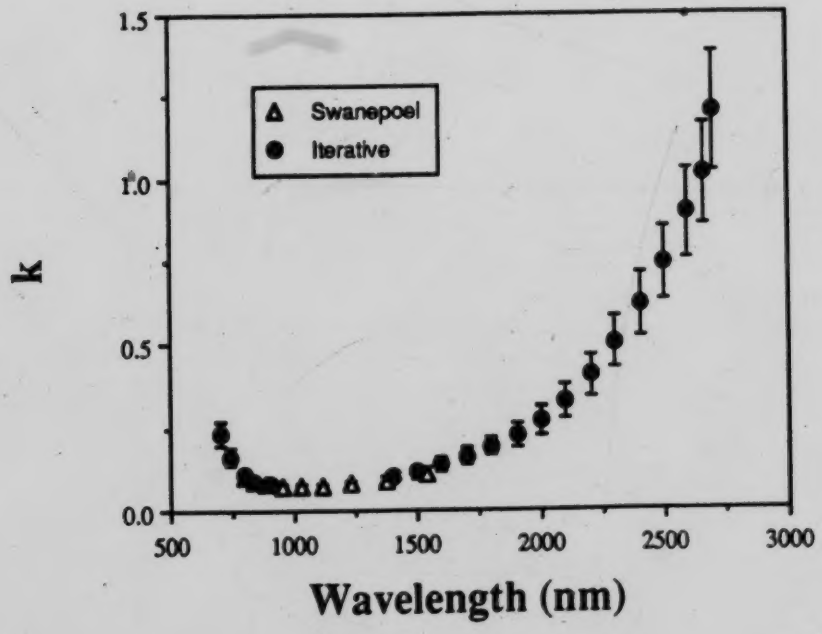

Figure 6.4 The extinction coefficient (k) of the film deposited at 90 W.

6.5) and the absorption of the film into account [81]. Since the absorption of the film is large, very little of the light can reflect from more than one interface, thus only the first two terms of these series are needed. By neglecting the higher terms, the maximum absolute error incurred is about 0.1 %. The equations for the transmission and reflection of the film/air stack reduce to:

$$T=(1-r_0)(1-r_1)(1-r_2)\, e^{-4\pi kd/\lambda} \tag{6.7}$$

$$R = r_0 + \left[(1-r_0)^2 r_1 + (1-r_0)^2 (1-r_1)^2 r_2\right] e^{-8\pi kd/\lambda} \tag{6.8}$$

where r_m is the reflection from each interface, given by:

$$r_m = \frac{(n_m - n_{m-1})^2 + (k_m - k_{m-1})^2}{(n_m + n_{m-1})^2 + (k_m + k_{m-1})^2} \tag{6.9}$$

and n_m, k_m are the optical constants of each layer.

Using the measured transmission and reflection spectra, the optical constants of the film were determined using an iterative technique. This technique calculates successive estimates of the reflection from the air/film interface. The iterations were continued until the calculated reflection from this first interface converged to a value that was less than 0.1 % of the last calculation. A detailed description of the algorithm follows:

1. T, R, the film thickness, and the optical constants of the substrate are known.
2. Set r_0=R and r_1=0 (Initial guess of the optical constants of the film).
3. Evaluate k using Eqn. 6.8.
4. Recalculate r_0 using the new value for k.
5. Evaluate n using Eqn 6.9.
6. Calculate a new r_0 using the new values of n and k.

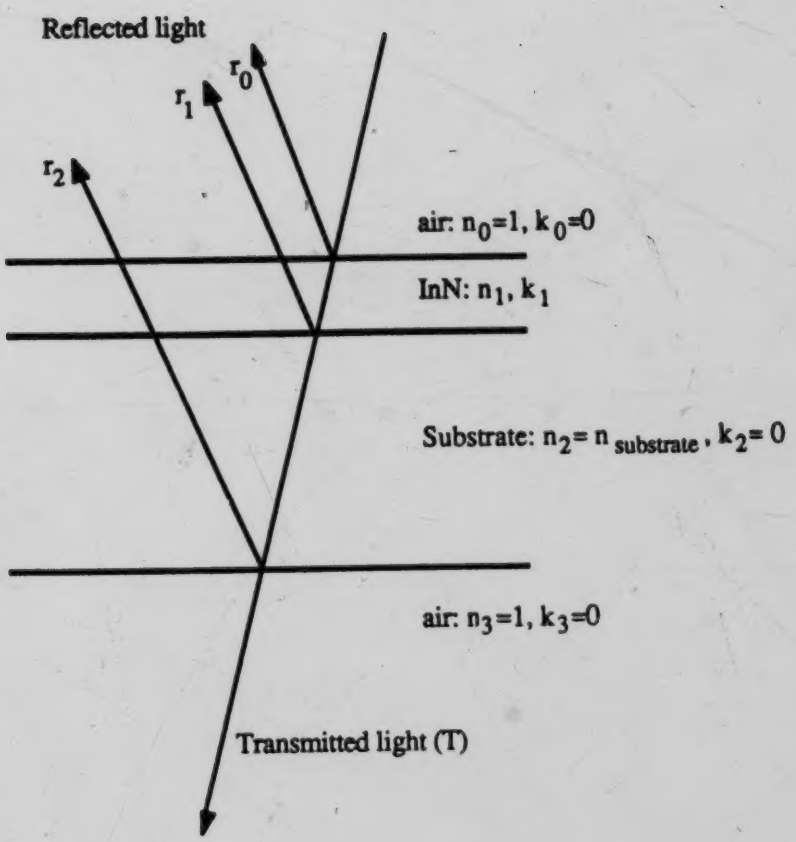

Figure 6.5 A schematic diagram of transmission and reflection from a thin film/substrate stack. The angles are exaggerated for clarity.

7. If the value of r_0 has not converged to within 0.1% of its previous value, repeat steps 3 through 6.

This technique converges in approximately 5 iterations. The optical constants for the 90 W film calculated using this technique are shown in Figures 6.3 and 6.4. The error in the optical constants is estimated to be 2 % in n and 11 % in k.

6.1.3 Discussion

Comparing the results from the two techniques (Figures 6.3 and 6.4), it is seen that in those regions where the results of the two techniques overlap, the values of the optical constants are within the stated error bounds of each. This agreement confirms that no systematic errors occurred in the measurements of the optical constants.

The optical constants of the two InN films deposited at 90 and 150 W are shown in Figures 6.6 and 6.7. There is very little difference between the optical constants of these two films. This is not surprising in light of the agreement of the results from the other characterization techniques, electrical properties, bandgap, and RBS measurements of the stoichiometry. Any small difference between the optical constants of the two films can be explained by a slight change in the composition of the films.

To compare values for the optical constants of InN with those of other authors [19,25,27], the reported values of the index of refraction were reviewed. Figure 6.8 shows a compilation of all reported values of n in the transparent region of the spectra, as well as those for the film deposited at 90 W. The reported values show that the general trends in n are similar, with the value lying between 2.5 to 3.1 in the 500 to 1100 nm region. However, the data has a fairly large amount of scatter. Since there are so few measurements of the index of refraction, one cannot say for certain which value is representative of InN.

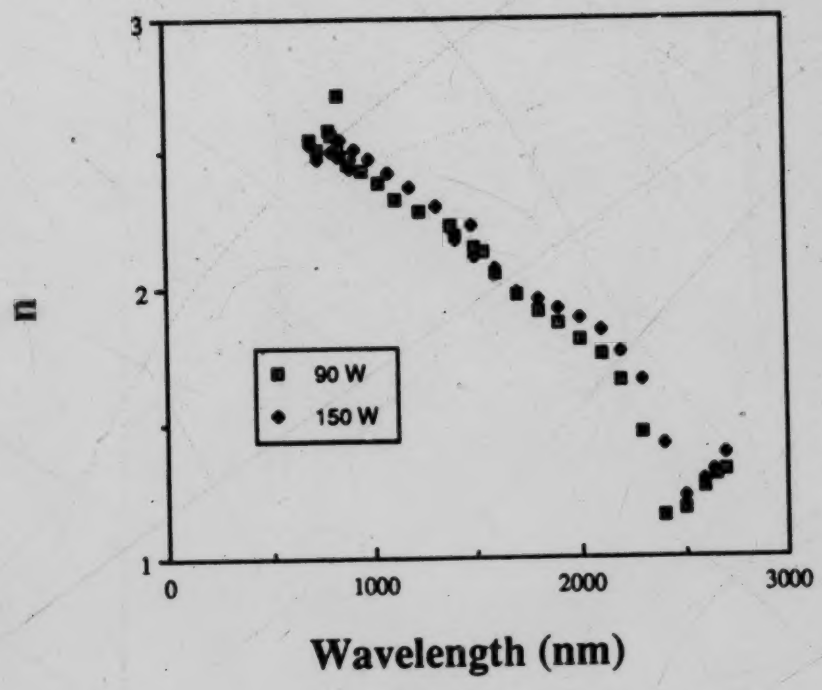

Figure 6.6 The index of refraction (n) of the InN films deposited at 90 and 150 W.

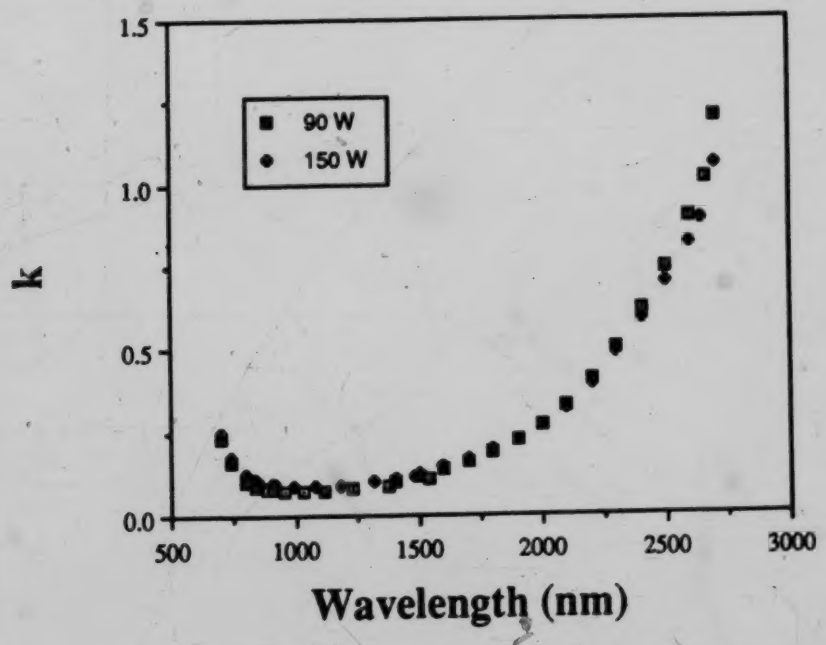

Figure 6.7 The extinction coefficient (k) of the InN films deposited at 90 and 150 W.

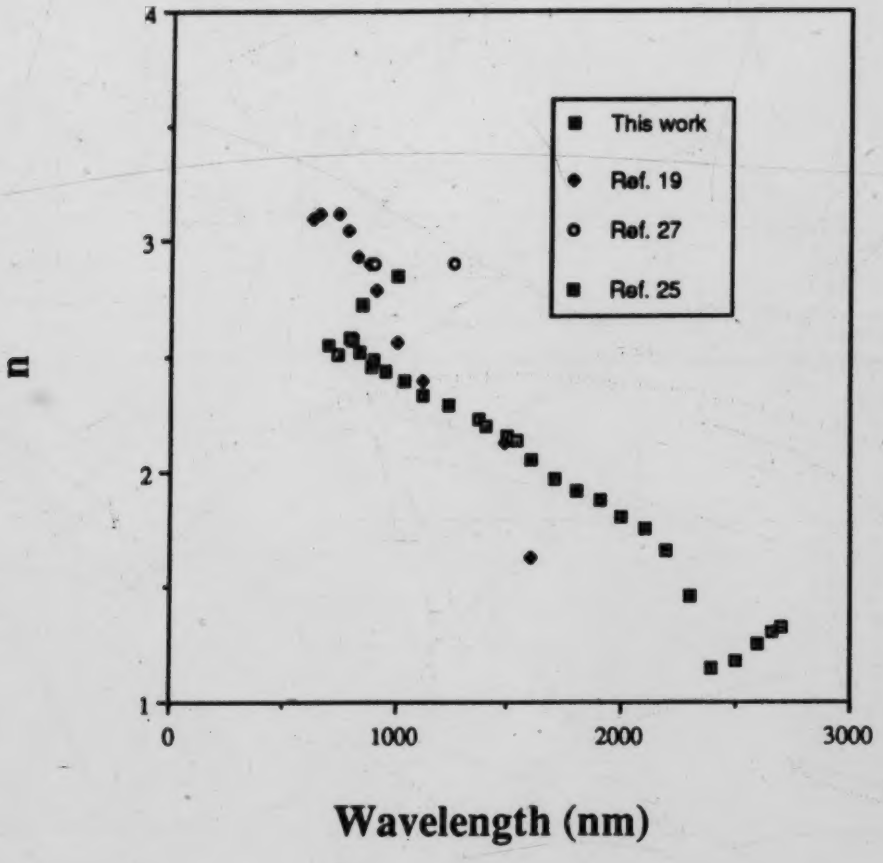

Figure 6.8 The reported values of the index of refraction (n) of InN. The values reported as representative of this work are for the film deposited at 90 W.

Comparing the systematic measurement of n, in the 700 to 2700 nm region for the 90 W film, with that of Tyagai et al., a significant difference is seen. Tyagai et al. measure a higher index of refraction at lower wavelengths while our data have their minima at much longer wavelengths. It is not clear why there is such differences between the two sets of data, although it could be related to the difference in the reported values of the bandgap. Tyagai et al. report a bandgap of 2.05 eV, which follows the empirical relation between the carrier concentration and bandgap determined by Tansley and Foley, while our value for the bandgap of 1.7 eV does not follow Tansley and Foley's relation.

6.2 Dielectric Constant of the Lattice (ε_∞)

One of the physical properties of a material that can be determined from the optical constants in the transparent region of a semiconductor is the dielectric constant of the lattice (ε_∞). This is the dielectric constant at frequencies high enough that the effects due to free electrons and from the phonon structure are negligible and only the lattice effects, remain [82].

It is difficult to measure ε_∞ at these high frequencies. However, the dielectric constant of the lattice can be determined from the index of refraction in a region of the optical spectra where the phonon and free electron effects are a minimum. At this minimum absorption region, the lattice dielectric constant is related to the index of refraction at the minimum absorption by $\varepsilon_\infty = n^2$ [82]. In semiconductors, the transparent region is such a region of low absorption. The index of refraction is chosen at the minimum value of k, as measured in the optical study. However, at this minimum absorption, there are some contributions from the free electrons and phonons on the value of ε_∞. Therefore, this technique does not yield the true lattice dielectric constant but only an approximate value. From the optical constants of InN (Figures 6.6 and 6.7), the index of refraction at the

minimum absorption (k) was found and used to calculate ε_∞ (Table 6.1). For the two InN films, the average lattice dielectric constant was found to be 5.8.

An alternative method of calculating ε_∞ is to use the Moss rule [29], which is an empirical relationship between the bandgap of a semiconductor and its index of refraction in the transparent region:

$$n^4 E_g = 77 \qquad 6.10$$

This equation has been shown to be valid for a large number of semiconductors with a range of n^4 between 30 and 440 [57]. Using this relationship and the bandgap determined for our samples (1.7 eV), the index of refraction is found to be 2.59 and the dielectric constant of the lattice is then 6.73 (Table 6.1).

Deposition Power	n at k_{min}	ε_∞
Moss Rule	2.59	6.73
90 W	2.39	5.71 ± 0.2
150 W	2.43	5.90 ± 0.2

Table 6.1 Determination of the dielectric constant of the lattice.

There are three values for ε_∞; the one reported by Tyagai et al. (9.3), the one determined from the Moss rule (6.73), and the one found using the optical constants of our films (5.8). This large variation in ε_∞ could be due to a number of effects. It has been shown that ε_∞ varies between 3 and 4, in In_2O_3, depending on the carrier concentration [54]. Thus the difference between the value reported by Tyagai et al. and ours could simply be a result of differences in the carrier concentrations or donor and acceptor concentrations. Also, the non zero absorption could have affected both the values of ε_∞

determined by Tyagai et al. and us. For the calculations of the optical constants in the infrared portion of the spectra, a value of ε_∞ =5.8 was used.

6.3 Determination of the Dominant Scattering Mechanism

From a quantum mechanical treatment of the Drude theory of free electrons it can be shown that the absorption at long wavelengths should fit a power law relation ($\alpha \propto \lambda^m$) [54,82,83], and that the exponent of the power law is related to the dominant scattering mechanism of the carriers. For example, m=1.5 for acoustic phonon scattering, and m=3.5 for ionized impurity scattering.

The absorption coefficient of the InN films was calculated from the optical extinction coefficient ($\alpha=4\pi k/\lambda$). Figure 6.9 shows the absorption in the region from 1900 to 2500 nm and the fitted power law expression. The exponent, m, that best fits the data is 3.51. This identifies the dominate scattering centre in these InN films is an ionized impurity [83]. This is not unexpected considering the large carrier concentrations and low mobilities of the electrons found in the films.

6.4 Infrared Reflectivity

Beyond 3 μm, the optical constants of InN could not be measured because the quartz substrates do not transmit light in this region. However, the optical constants of heavily doped semiconductor thin films (ie. ZnO [84], In_2O_3 [54]) have been quite well modelled in this region using the Drude theory of free electrons. In this section, the infrared reflectivity of the InN films was determined experimentally (2.5 to 20 μm), and using the Drude theory of free electrons and the optical constants of quartz, the reflectivity of the film/substrate structure was modelled. By fitting the modelled reflectivity to the experimental reflectivity, the effective mass of the electrons in the InN thin film was determined.

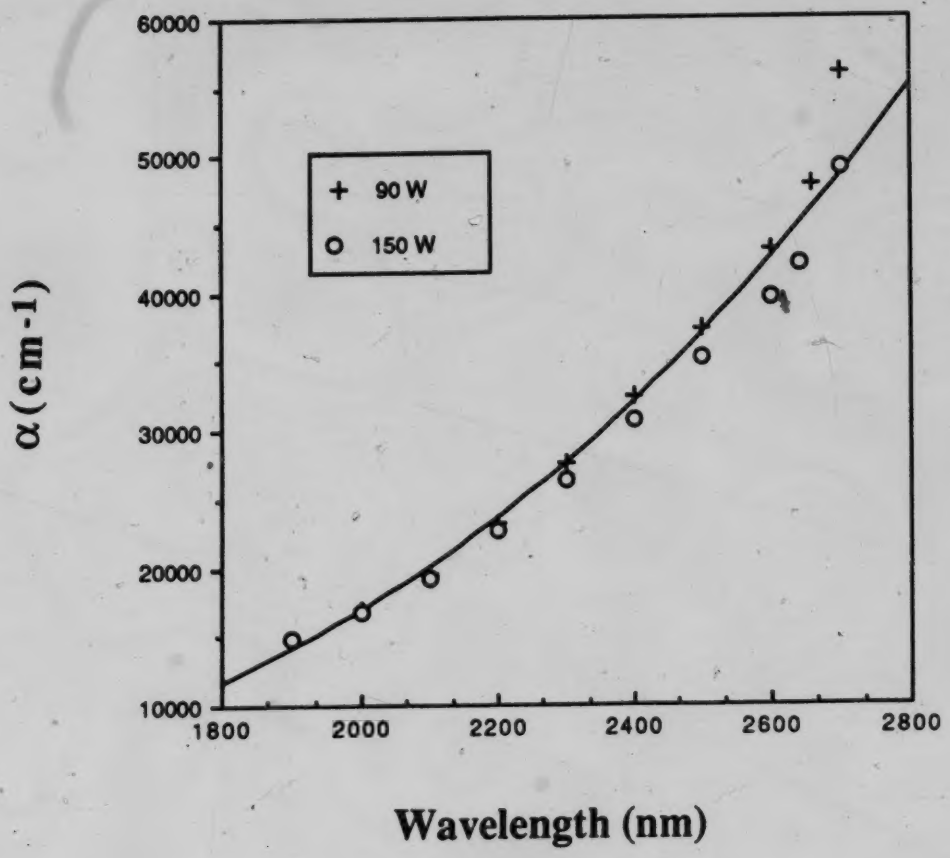

Figure 6.9 The absorption of the 90 and 150 W films and a power law (λ^m) fit to the data. The best fit of m=3.51 suggests that ionized impurities are the dominant scattering mechanism.

6.4.1 Drude theory of free electrons

In the infrared portion of the spectra, the optical properties of a material are dominated by the phonon structure (Restrahlen bands) and by free electron effects. In heavily doped (degenerate) semiconductors the effects of the phonon structure are overcome by the free electron effects. Typically, this produces a high reflectivity which is a smooth function of wavelength, with none of the structure associated with phonons [84]. Since the two InN films, deposited at 90 and 150 W, have a carrier concentration in the 10^{20} cm^{-3} range, the free electron effects in these films should dominate and the phonon structure of InN should have little or no effect on the measured infrared reflectivity.

In a material with a large concentration of carriers, such as heavily doped semiconductors, the carriers in the material can be assumed to be a sea of free carriers. The optical constants of such a material are derived by looking at the effect of an impinging electromagnetic wave on this sea of free electrons [85]. To account for the effects of the lattice and the imperfections in the material, one assumes that the motions of the electrons are damped by collisions with lattice imperfections (scattering centres) and that the mass of the carrier is modified by the presence of the lattice (carrier effective mass). This derivation yields a simple differential equation which also describes the motion of a damped harmonic oscillator. This approach was orginally developed by P. Drude and is known as the Drude theory of free electrons [85].

The derivation of the optical constants using the Drude theory of free electrons is simplified by using the dielectric constant, rather than the optical constants, n and k, of the material, where the dielectric constant is given by: $\varepsilon = \varepsilon_1 + i\,\varepsilon_2$. The dielectric constant and the optical constants are related by the simple expressions:

$$\varepsilon_1 = n^2 - k^2 \qquad (6.11)$$

$$\varepsilon_2 = 2nk \tag{6.12}$$

Solving the Drude equations in one dimension yields two equations that provide the dielectric constant of the film [54]:

$$\varepsilon_1 = \varepsilon_\infty - \frac{\omega_n^2}{\omega^2 + \gamma^2} \tag{6.13}$$

$$\varepsilon_2 = (\gamma/\omega)\left[\frac{\omega_n^2}{\omega^2 + \gamma^2}\right] \tag{6.14}$$

where:

$$\omega_n^2 = \frac{n_e q^2}{\varepsilon_0 m_e^*} \tag{6.15}$$

and n_e is the carrier concentration, q is the charge of an electron, ε_0 is the static dielectric constant, m_e^* is the effective mass of the carrier, ω is the frequency of the incident light, and γ is the recipocal relaxation time.

The unknowns in these equations are: the carrier concentration (n_e), the dielectric constant of the lattice (ε_∞), the reciprocal relaxation time (γ), and the effective mass of the carriers (m^*_e). The carrier concentration and ε_∞ have already been determined for the two InN films, while γ is related to the mean time between scattering events (collisions) of the carriers. In a simplified theory, γ is related to the carrier effective mass and the carrier mobility. However, this assumes that the velocities of a carrier before and after a collision are not related. This assumption is not necessarily correct and is not true if scattering from ionized impurities occurs in the material. As was discussed earlier, the dominant

scattering in these films is most likely caused by ionized impurities. Thus γ must be determined in another manner.

Another way of determining γ is from experimental measurements of the plasma frequency. The plasma frequency (ω_p) is defined as the frequency at which $\varepsilon_1=0$, and this can be determined using the measured optical constants of the films. At the plasma frequency, equation 6.13 can be rewritten as:

$$\omega_p^2 = \frac{\omega_n^2}{\varepsilon_\infty} - \gamma^2 \qquad (6.16)$$

The plasma frequency of the two InN films was determined from extrapolating the measured n and k until the frequencies at which $n^2-k^2=0$, were determined (Table 6.2). Using the plasma frequency (ω_p), ε_∞, the carrier concentration (n_e), and equation 6.16, γ was determined as a function of the electron effective mass.

6.4.2 Comparison Between the Modelled and Experimental Infrared Reflectivity

The infrared reflectivity of the InN films was measured in the region 2.5 to 20 μm using a Perkin Elmer model 457 infrared spectrophotometer. A gold film deposited on a glass substrate was used as the reflection standard in these measurements. The measurements were corrected for the 98% reflectivity of the gold in this spectral region [86]. The measured reflectivities of the 90 W and 150 W films is shown in Figures 6.10 and 6.11. The films did not show any obvious evidence of phonon absorption bands. Therefore the assumption to use only the free electron theory in calculating the optical properties appears to be valid.

The reflectivity of the film/substrate stack was calculated using the optical constants of the film as determined by the Drude theory and the tabulated optical constants for

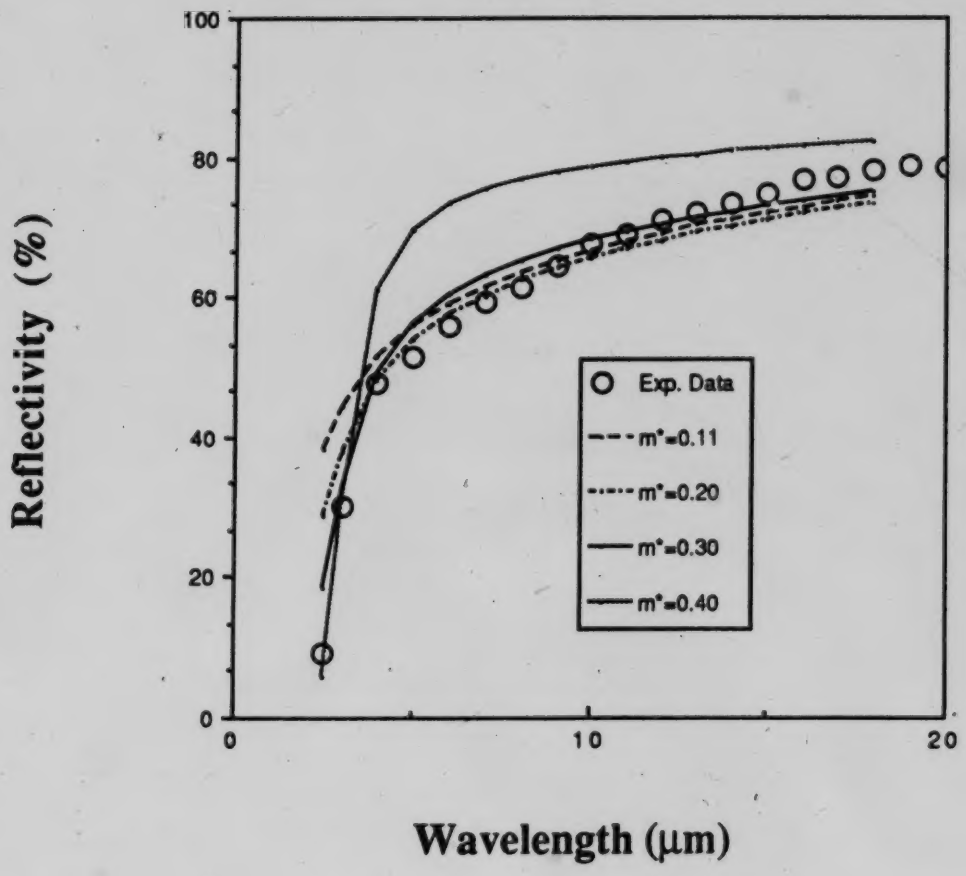

Figure 6.10 The measured and modelled infrared reflectivity of the film deposited at 90 W showing the fit of various electron effective masses.

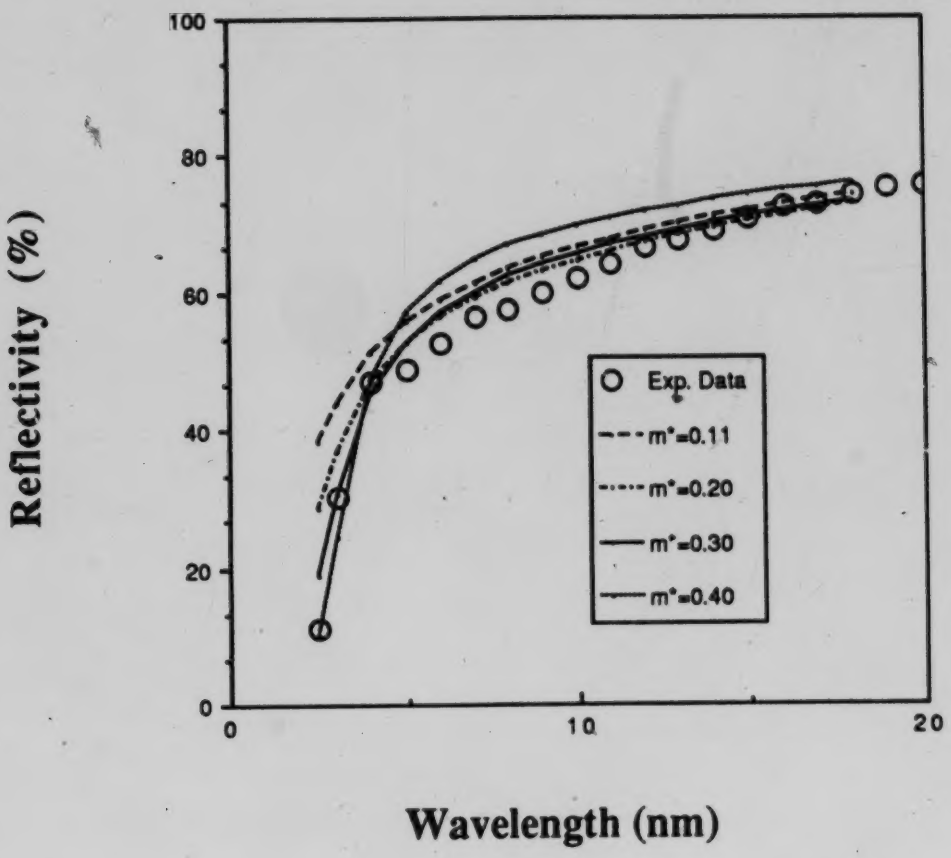

Figure 6.11 The measured and modelled infrared reflectivity of the film deposited at 150 W film showing the fits of various electron effective masses.

quartz [79]. The transmission and reflection spectra for a film/substrate stack using the optical constants of the modelled InN and quartz substrate were calculated using an impedance matching technique at the various interfaces in the stack [81].

The reflectivity of the InN film/quartz substrate stack was calculated using a number of different effective masses for both films. Figures 6.10 and 6.11 show the fit to various effective masses between 0.11 and 0.4 m_e. The best fit of the infrared reflectivity for both films gave an electron effective mass of about 0.3.

There is a large difference between the effective mass determined by Tyagai et al. [19] (m_e^*=0.11) and that reported here. The theoretical calculation of Foley and Tansley [29] (m_e^*=0.12) supports the measurement of Tyagai et al. It is unclear why our value of the effective mass is larger than that of Tyagai et al., especially since they determined m_e^* using a technique very similar to ours. The disagreement could be related to the other differences between our work and Tyagai et al.'s that have been mentioned, such as the bandgap and the index of refraction. In addition, our significantly higher electron effective mass could be a result of the impurity state that has been proposed as the source of the 1.7 ev band gap [1], or a result of changes in the effective mass caused by the filling of the conduction band in this degenerate material [82].

6.5 Mean Free Path

The mean free path of electrons between scattering collisions in the InN films can be calculated now that γ and the effective mass of the electron in these samples has been determined. The mean free path of the electrons in the sample is given by:

$$l = v_f t = v_f/\gamma \qquad (6.17)$$

where l is the mean free path, t is the time between collisions, and v_f is the electron velocity in a solid, which is given by the Fermi velocity [87]:

$$v_f = \frac{h^2}{(2\pi)^2 m_e^*} (3\pi^2 n_e)^{1/3} \qquad (6.18)$$

Assuming an electron effective mass of 0.3, the mean free path for the two samples was calculated to be between 1 and 2 nm (Table 6.2). This is significantly smaller than the crystallite size calculated from the XRD data (20 nm) and implies that the scattering centres that dominate the carrier mobility in the InN samples are found throughout the film, not just at grain boundaries.

Deposition Power	ω_p (nm)	γ (s^{-1})	v_f (cm/s)	mfp (nm)
90 W	2800	4.53×10^{14}	8.5×10^7	1.9
150 W	3000	5.35×10^{14}	8.6×10^7	1.6

Table 6.2 Various parameters of the InN films.

6.6 Summary

The optical constants of InN were determined in the region from 700 to 2700 nm for two films deposited at 90 and 150 W. The optical constants, n and k, for both films were very similar, however they differed significantly from those reported by Tyagai et al.. Using these optical constants and the electrical properties of the InN thin films, the infrared reflectivity of the films was modelled using the Drude theory of free electrons. By fitting the infrared reflectivity to the modelled reflectivity, the effective mass of the

electrons was found to be $0.3m_e$. This is significantly higher than that reported in the only other experimental determination (m_e=0.11) [19].

Chapter 7

Conclusions

The initial goal of this work was to reproduce the high electron mobility InN films reported by Tansley and Foley [3,4]. Characterization of some early InN films showed that the films had a low electron mobility and contained significant amounts of oxygen throughout the film bulk [17]. To try to understand these results, a study of the reactivity of indium with the various gases in the sputter chamber was undertaken. This study concluded that InN is formed, during reactive sputtering, by the reaction of indium with atomic or excited nitrogen and not with N_2 sputter gas. Secondly, the indium would strongly react with residual oxygen in the sputter chamber. To reduce the possible contamination of the InN films by this residual oxygen, the base pressure of the sputter chamber was reduced by a factor of 20 by repairing air leaks and by reducing the outgassing of water vapour from the interior walls of the system.

At these low base pressures a series of films were deposited at various deposition powers and sputter gas pressures. These films were characterized using XRD, bandgap measurements, and Hall probe studies. The films were found to be polycrystalline InN with a direct bandgap of 1.7 eV. The Hall probe study showed no improvement in the electron mobility compared to the initial work, that is, electron mobilities in the range of 6 to 10 cm^2/Vs. The stoichiometry of two of these films was measured using RBS and was found to contain 10 to 11 at. % oxygen throughout the bulk of the film. This is also similar to the initial films. Thus the reduction in the base pressure did not appear to affect the properties of the InN films. From a literature search it was found that oxygen contamination of nitrides is a common problem and that a majority of the oxygen seen throughout the film bulk could be due to oxidation of the surface of the columnar structure and not incorporated during deposition.

However, oxidation of the column surfaces does not explain the low mobilities that are observed in these InN films. To explain the low mobilities, it was proposed that the oxygen which was incorporated into the film during deposition acted as both an electron donor and as a scattering centre. The supporting evidence is twofold: studies of AlN and GaP have found that oxygen acts as a deep donor state in these materials and, from the optical study of InN, it was found that the dominant scattering centre in these films was an ionized impurity.

The optical constants of the InN films deposited at the low base pressures were determined in the visible and near infrared regions using both an iterative technique and the technique developed by Swanepoel. The optical constants were used to determine the lattice dielectric constant and the electron relaxation time. These two parameters were then used in modelling the optical reflectivity of the InN film in the 2.5 to 20 μm region using the Drude theory of free electrons and the optical constants for quartz. By fitting the modelled reflectivity of the films to the measured reflectivity, the effective mass of the electrons was found to be 0.3 m_e.

Since the initial goal of producing high mobility films was not met, it is apparent that much work still needs to be done. From this research, it appears that the mobility of InN is limited by the concentration of nitrogen vacancies and oxygen impurities in the films. To reduce both of these effects, the amount of atomic nitrogen at the growing film surface must be dramatically increased, which would in turn increase the electron mobility in the film. This can be done using a number of different techniques such as, for example, the use of secondary discharges near or at the substrate [17,32]. Another method of increasing the atomic nitrogen concentration is to add gases to the sputter gas which increase the rate at which atomic nitrogen is produced from N_2. Neon [88] has been suggested as a gas which might be used for this application.

To directly determine where and how the oxygen is bound in the films requires the use of surface analysis tools that can be used to probe very small regions of the film. Mico-spot Auger or TEM studies using convergent beam electron diffraction (CBED) and electron energy loss spectroscopy (EELS) are techniques which could be used in such a study.

Many mysteries still exist with InN, some of which are mentioned in this thesis. Two central questions that remain are: 1) what causes the differences between the optical constants and the electron effective mass reported by Tyagai et al. and those reported here and 2) what is the actual cause of the low electron mobilities and how can this problem be overcome to make the deposition of high mobility films possible. It will be the task of future researchers to answer these questions and I hope that this work has made their job a little easier.

References

1. T.L. Tansley and C.P. Foley, "Optical band gap of indium nitride," J. Appl. Phys. **59 (9)**, 3241 (1986).

2. O. Takai, "Microwave ion plating technique," in *Proc. 7th ICVM* (Tokyo, Japan) p 865 (1982).

3. T.L. Tansley and C.P. Foley, "Electron mobility in indium nitride," Electron. Lett. **20**, 1066 (1984).

4. T.L. Tansley and C.P. Foley, "Polycrystalline indium nitride films," in *Semi-Insulating III-V Materials*, edited by D.L. Look and J.S. Blakemore (Shiva, London, 1984) p. 497.

5. J.S. Blakemore, "Semiconducting and other major properties of gallium arsenide," J. Appl. Phys. **53** (10), R123 (1982).

6. C.P Foley and T.L. Tansley, "Morphology and structure of indium nitride films," Appl. Surf. Sci. **22/23**, 663 (1985).

7. F.S. Ohuchi and P.E. Rossel, "AlN thin films with crystallographic orientations and their microstructure," J. Vac. Sci. Technol. A **5** (4) 1630 (1987).

8. A. Kawabata, "Fabrication techniques and properties of piezoelectric thin films of ZnO and AlN," Japanese J. Appl. Phys **23** Supp. 23-1, 17 (1984).

9. T. Shiosaki, K. Harada, and A.K. Kawabata, "Low temperature growth of piezoelectric AlN and its optical and acoustical properties," Japanese J. Appl. Phys. **21** Supp 21-3, 69 (1982).

10. I. Akasaki, H. Amano, K. Hiramatsu, and N. Sawaki, "High efficency blue LED utilizing GaN film with AlN buffer layer grown by MOVPE," Inst. Phys. Conf. Ser. no. 91: Chapter 7 p 633 (1988).

11. Y. Koide, H. Itoh, N. Sawaki, and I. Akasaki, "Epitaxial growth and properties of $Al_xGa_{1-x}N$ by MOVPE," J. Eletrochem Soc. **133** (9), 1956 (1986).

12. U. Zhumakulov, "The edge of fundamental absorption and photoluminescene of $Ga_xAl_{1-x}N$ epitaxial layers," Solid State Comm. **58** (6), 367 (1986).

13. S. Yoshida, S. Misawa, and S. Gonda, "Properties of $Al_xGa_{1-x}N$ films prepared by reactive molecular beam epitaxy," J. Appl. Phys. 53 (10), 6844 (1982).

14. K. Osamura, K. Nakajima, and Y. Murakami, "Fundamental absorption edge in GaN, InN and their alloys," Solid State Comm. **11**, 617 (1972).

15. K. Osamura, S Naka, and Y. Murakami, "Preparation and optical properties of $Ga_{1-x}In_xN$ Thin films," J. Appl. Phys. **46** (8), 3432 (1975).

16. K.L. Westra and M.J. Brett, unpublished (1988).

17. K.L. Westra, R.P.W. Lawson, and M.J. Brett, " The effects of oxygen contamination on the properties of reactively sputtered indium nitride thin films," J. Vac. Sci. Technol. A **6** (3), 1730 (1988).

18. H. Hahn and R. Jusa, Z. Anorg. Allg. Chem. **244**, 111 (1940).

19. V.A. Tyagai, A.M. Evstigneev, A.N. Krasiko, A.F. Andreeva, and V.Ya. Malakhov, " Optical properties of indium nitride films," Sov. Phys. Semicond. **11** (11), 1257 (1978).

20. L.A. Marasina, I.G. Pichugin, and M. Tlaczala, "Preparation of InN epitaxial layers in $InCl_3$-NH_3 system, " Kristall und Technik **12 (6)**, 541 (1977).

21. J.W. Trainor and K. Rose, " Some properties of InN films prepared by reactive evaporation," Journal of Electronic Materials **3 (4)**, 821 (1974).

22. G.V. Samsonov and A.F. Andreeva, "Physical properties of indium nitride films," Science of Sintering **12 (3)**, 155 (1980).

23. O. Takai, J. Ebisawa, and Y. Hisamatsu, "Properties of indium nitride films prepared by reactive ion plating," in *Proc. 7th ICVM* (Tokyo, Japan) p. 137 (1982).

24. N. Puychevrier and M. Menoret, "Synthesis of III-V semiconductor nitrides by reactive cathodic sputtering," Thin Solid Films **36**, 141 (1976).

25. B.R. Natarajan, A.H. Eltoukhy, J.E. Greene, and T.L. Barr, "Mechanisms of reactive sputtering of indium I: Growth of InN in mixed Ar-N_2 Discharges," Thin Solid Films **69**, 201 (1980).

26. R.D. Jones, *The Growth and Characterization of III-Nitrogen Compounds*, PhD thesis, Rensselaer Polytechnic Institute (1986).

27. H.J. Hovel and J.J. Cuomo, "Electrical and optical properties of rf-sputtered GaN and InN," Appl. Phys. Lett. **20**, 71 (1972).

28. Brian T. Sullivan, R.R. Parsons, K.L. Westra, and M.J. Brett, " Optical properties and microstructure of reactively sputtered indium nitride thin films," J. Appl. Phys. in press.

29. C.P Foley and T.L Tansley, "Pseudopotential band structure of indium nitride," Phys. Rev. B **33 (2)**, 1430 (1986).

30. S.N. Grinyaev. Y. Va. Malakhov, and V.A. Chaldyshev, "Calculation of the band structure of GaN and InN using the pseudopotential method," Sov. Phys.J. **29** (4) 311 (1986).

31. D.W. Jenkins, R.D. Hong, and J.D. Dow, "Band structure of InN,' Superlattices and Microstructure **3** (4) 365 (1987).

32. B. Chapman, *Glow Discharge Physics: Sputtering and Plasma Etching* (John Wiley and Sons, New York, 1980).

33. W.D. Westwood and J.J. Cuomo, in *AVS Short Course Notes: Sputter Deposition and Ion Beam Processes*, (American Vacuum Society) Chapter 5 p11.

34. J.E. Greene, "Epitaxial crystal growth by sputter deposition: Applications to semiconductors. Part 2," Crit. Rev. Solid State Sci. **11** (3), 189 (1982).

35. J.A. Thornton and A.S. Penfold in*Thin Films Processes* p 109, ed. J.L. Vossen and W. Kern (Academic, Orlando, 1978).

36. H.F. Winters and E. Kay, "Influence of surface absorption characteristics on reactively sputtered films grown in the biased ans unbiased modes," J. Appl. Phys. **43**, 794 (1972).

37. R.S. Boikess and E. Edelson, *Chemical Principles* (Harper and Row, New York, 1978).

38. V.S. Schiller, V. Heisig, K. Steinfelder, J. Strumpfel, and W. Sieber, "Reactive DC high rate sputtering with the magnetron/plasmatron for industrial applications," Vakuum-Technik 30, **3** (1981).

39. R. McMahon, J. Affinto, and R.R. Parsons, "Voltage controlled, reactive planar magnetron sputtering of AlN thin films," J. Vac. Sci. Technol. 20 (3) 376 (1982).

40. J.F. O'Hanlon, *A User's Guide to Vacuum Technology*, (John Wiley and Sons, New York, 1980).

41. *Handbook of Chemistry and Physics, 1st Student Edition*, Ed. R.C. Weast (CRC Press, Boca Raton Florida, 1988).

42. B. Chapman, *Glow Discharge Physics: Sputtering and Plasma Eching*, p 147 (John Wiley and Sons, New York, 1980).

43. M.J. Brett, personal communication.

44. J.F. O'Hanlon, *A User's Guide to Vacuum Technology*, p 280, (John Wiley and Sons, New York, 1980).

45. J.A. Thorton "The microstructure of sputter deposited coating," J. Vac. Sci. Technol. A 4 (6), 3059 (1986).

46. B.A. Movchan and A.V. Demchishin, Phys. Met. Metallogr. 28, 83 (1969).

47. J.A. Thorton ,"High rate thick film growth," Ann. Rev. Mater. Sci. 7, 239 (1977).

48. J.A. Thorton, "Structure-zone models of thin films," in *Modeling of Optical Thin Films*, M.R. Jacobson Ed. (SPIE, Bellingham Wash., 1987).

49. D.W. Hoffman and J.A. Thorton, "Compressive stress and inert gas in Mo films sputtered from a cylindrical post magnetron with Ne, Ar, Kr, and Xe," J. Vac. Sci Technol. 17 (1) 380 1980.

50. T.C. Huang, G. Lim, F. Parmigiana, and E. Kay, "Effect of ion bombardment during deposition on the x-ray microstructure of thin silver films," J. Vac. Sci. Technol. A **3** (6), 2161 (1985).

51. B.D. Cullity, *Elements of X-Ray Diffractionn, 2nd Edition* (Addison-Wesley, Reading Massachuetts, 1978).

52. M.J. Brett and R.R. Parsons, "Structural properties of nonstoichiometric zinc oxide films," J. Mat. Sci. **22** 3611 (1987).

53. V.V. Sobolev, S. G. Kroitoru, A.F. Andreeva, and V. Ya. Malakhov, "Reflection spectra of indium nitride," Sov. Phys. Semicond. **13** (4), 485 (1979).

54. I. Hamburg and C.G. Granquist, " Evaporated Sn-doped In_2O_3: Basic optical properties and applications to energy-efficient windows," J. Appl. Phys. **60** (11), R123 (1986).

55. B.E. Sernelius, K.F. Berggren, Z.C. Jin, I. Hamberg, and C.G. Granquist, "Band-gap tailoring of ZnO by means of heavy Al doping,' Phys. Rev. B **37** (17), 10244 (1988).

56. I. Hamberg, C.G. Granquist, K.F. Berggren, B.E. Serelius, and L. Engstrom, "Band-gap widening in heavily Sn-doped In_2O_3," Phys Rev. B **30** (6), 3240 (1984).

57. J.I. Pankove, *Optical Processes on Semiconductors,* (Dover, New York, 1975).

58. A.H. Roth, J.B. Webb and D.F. Williams, "Absorption edge shift in ZnO thin films at higher carrier densities," Solid State Comm. **39**, 1269 (1981).

59. F. Urbach, "The long-wavelength edge of photographic sensitivity and the electron absorption of solids," Phys. Rev. Lett. **92** 1324 (1953).

60. M.A. Logan, Bell System Tech. J. **40**, 885 (1961).

61. R.A. Smith, *Semiconductors*, 2nd ed. (Cambridge University Press, Cambridge, 1979).

62. W.K. Chu, J.W. Mayer, and M.A. Nicolet, *Backscattering Spectrometry*, (Academic Press, New York, 1978).

63. E.O. Ristolainen, J.M. Molarius, A.S. Korhonen, and V.K. Lindroos, "A study of nitrogen rich titanium and ziconium nitride films" J. Vac. Sci. Technol. B **5** (4), 2184 (1987).

64. T. Brat, N. Parikh, A.K. Sinha, J. Poole, and C. Wickersham, "Characterization of titanium nitride films sputter deposited from a high purity titanium nitride target," J. Vac. Sci. Technol. B **5** (6), 1741 (1987).

65. T.P. Thorpe, W.T. Elam, and A. Morrish, "Correlation of microstructure and composition of sputtered titanium nitride films with electrical and optical properties," J. Vac. Sci. Technol. A 5 (4), 1652 (1987).

66. D.S. Williams, F.A. Baiocchi, R.C. Beairsto, J.M. Brown, R.V. Knoella and S.P. Murarka, "Nitrogen, oxygen, and argon incorperation during reactive sputter deposition of titanium nitride," J. Vac. Sci. Technol. B **5** (6), 1723 (1987).

67. D.S. Yee, J.J. Cuomo, M.A. Frisch, and D.P.E. Smith, "Reactive radio frequency sputter deposition of higher nitrides of titanium, zirconium, and hafnium," J. Vac. Sci. Technol. A **4** (3) 381 (1986).

68. B. Mehrotra and J. Stimmell, "Properties of direct current magnetron reactively sputtered TaN," J. Vac. Sci. Technol. B 5 (6), 1736 (1987).

69. C.P Foley and J. Lyngdal, "Analysis of indium nitride surface oxidation," J. Vac. Sci. Technol. A 5 (4), 1708 (1987).

70. O. Takai, J. Ebisawa, and Y. Hisamatsu, "Preparation of indium nitride films by R.F. reactive ion plating," in *Proc. 7th ICVM* (Tokyo, Japan) p. 129 (1982).

71. B.R. Natarajan, A.H. Eltoukhy, J.E. Greene, and T.L. Barr, "Mechanisms of reactive sputtering of indium II: Growth of indium oxynitride in mixed N_2-O_2 discharges," Thin Solid Films **69**, 217 (1980).

72. J. Pastrnak, S. Pacesova, and L. Roskovcova, "Luminescent properties of the oxygen impurity centres in AlN," Czech. J. Phys. B **24**, 1149 (1974).

73. I. Tale and J. Rosa, "Fractional glow technique spectroscopy of traps in heavily doped AlN:O," Phys. Stat. Sol. (a) 86, 319 (1984).

74. D.F. Neely, T.L. Tansley, and C.P. Foley, "A low cost R.F. sputtering system for the production of thin films," in *2nd Applied Physics Conference of the Australian Institute of Physics* , p. 296 (1981).

75. T.L. Tansley and C.P. Foley, "Infrared absorption in indium nitride," J. Appl. Phys. **60 (6)**, 2092 (1986).

76. R. Swanepoel, " Determination of the thickness and optical constants of amorphous silicon," J. Phys. E **16**, 1214 (1983).

77. M.J. Brett, "Stoichiometry control mechanisms of bias sputtered zinc oxide films," Phd Thesis, University of British Columbia (1985).

78. I.H. Malitson, "Interspecimen comparison of the refractive index of fused silica," J. Opt. Soc. Amer. **55** (10), 1205 (1965).

79. H.R. Philipp, "The infrared optical properties of SiO_2 and SiO_2 layers on silicon," J. Appl. Phys. **50** (2), 1053 (1979).

80. J.C. Manifacier, J. Gasiot, and J.P. Fillard, " A simple method for the determination of the optical constants n, k, and the thickness of a weakly absorbing thin film," J. Phys. E **9**, 1002 (1976).

81. H.A. Macleod, *Thin Film Optical Filters*, p 19 (American Elsevier, New York, 1969).

82. B. Jensen "The quantum extension of the Drude-Zener theory in polar semiconductors," in *Handbook of Optical Constants of Solids*, ed. E.D. Palik (Academic Press Inc., New York, 1985).

83. R. von Baltz and W. Escher, "Quantum theory of free carrier absorption," Phys. Stat. Sol. (B) **51**, 499 (1972).

84. M.J. Brett and R.R. Parsons, "Optical properties of nonstoichiometric zinc oxide deposited by bias sputtering,' J. Vac. Sci. Technol. A **4** (3) 423 (1986).

85. R.E. Hummel, *Electronic Properties of Materials*, (Springer-Verlag, Berlin,1985).

86. *Handbook of Optics*, Ed. W.G. Driseoll and W. Vaughan p 7-148 (MacGraw-Hill, New York, 1978).

87. N.W. Ashcroft and N.D. Mermin, *Solid State Physics*, (Saunders College, Philadelphia, 1976).

88. K.J. Huber and C.R. Aita, "Resistivity changes and phase evolution in W-N films sputter deposited in Ne-N_2 and Ar-N_2 discharges," J. Vac. Sci. Technol. A 6 (3) 1717 (1988).

Appendix

The Variation of Film Properties with Deposition Conditions

The variation of the film properties, particularly the electron concentration and mobility, were studied as a function of the target power and the total sputter gas pressure. These two deposition conditions were chosen because they can be easily varied and because both can be expected to affect the deposition rate and the concentration of atomic and excited nitrogen in the discharge. These, in turn, should affect the film stoichiometry and the properties of the resultant films. In this study, the deposition power was varied from 30 to 210 W at constant gas pressure and flow, while the sputter gas pressure was varied from 2 to 12 mtorr at constant target power.

In the first experiment, the target power was varied from 30 to 210 W, while the other sputter conditions remained constant as shown in Table 3.3. The deposition rate was found to monotonically increase with increasing target power (Figure A.1). There were no sudden changes as would be expected if the target/gas system had passed through a hysteresis point [38,39]. This lack of hysteresis further supported the conclusions of the heat of formation study in Chapter 2, that the surface of the indium target was never completely covered by a nitride layer. Over the range of target powers used in these experiments, the deposition rate increased by a factor of 5, which is a significant variation. The electron concentration and mobility, as well as the bandgap, were determined for these films. The results of the electrical characterization (Figure A.2) showed only small variations between the films deposited at the various powers. The bandgap (Table A.1) also did not change significantly over the range of target powers.

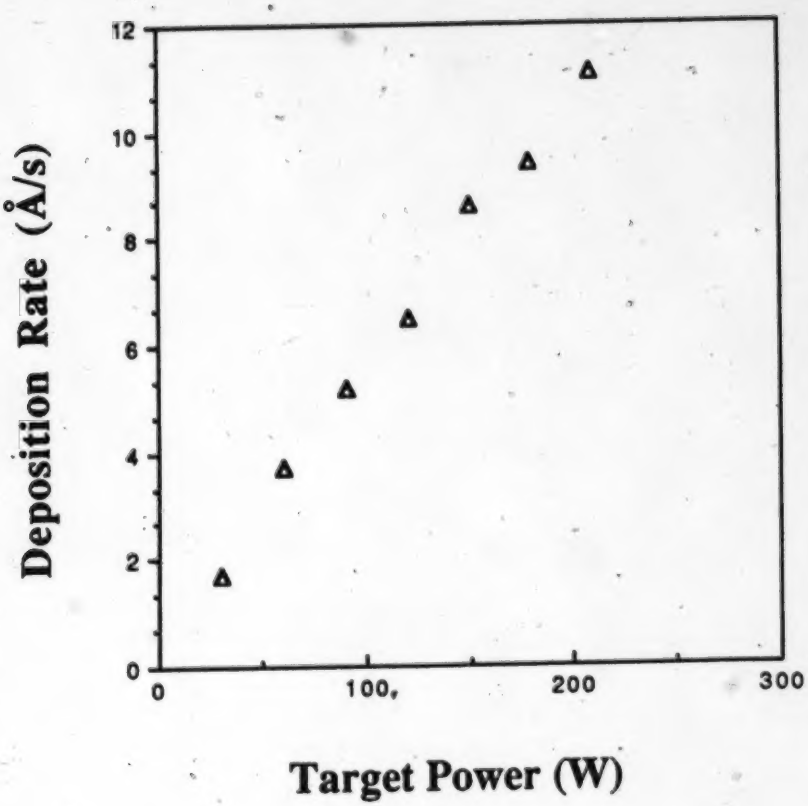

Figure A.1 Deposition rate of InN as a function of target power.

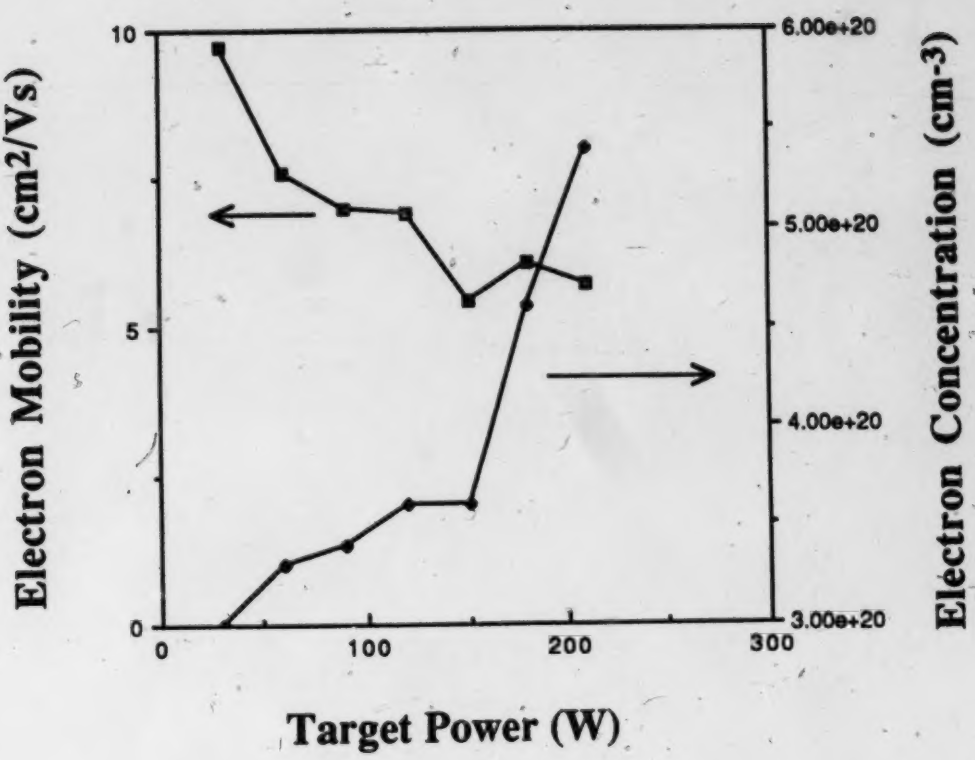

Figure A.2 Electron mobility and concentration as a function of target power.

The small variations in the film properties with deposition power can be explained by small changes in the stoichiometry of the films caused by the variations in the deposition rate. For example, the decrease in the electron mobility and the bandgap of these films with increasing deposition power could be caused by a decrease in the nitrogen content of the film, which is a result of an increase in the deposition rate.

Deposition Power (W)	Bandgap (eV)
30	1.70
90	1.70
150	1.70
180	1.69

Table A.1 The bandgap of InN measured as a function of the target power.

In the second set of experiments, the total nitrogen pressure during sputtering was varied from 2 to 12 mtorr at a constant target power of 90 W. The increased sputter gas pressure will affect the concentration of reactive nitrogen species near the surface of the growing film. In these experiments, there was no evidence of the indium target surface composition varying with the increased sputter gas pressure, that is, there is no evidence of target hysteresis effects occuring. The electrical properties of the films varied only slightly (Figure A.3), but remained within the bounds seen in the other experiments reported in this thesis. The trends in the electron concentration and mobility cannot be as easily explained as the results for the target power experiments, but they are still probably related to changes in the stoichiometry. It is unclear why the electron mobility decreases with increased N_2 pressure, since it would be expected that the amount of atomic and excited nitrogen species in the discharge will increase, if the total number of nitrogen atoms in the discharge increases.

A general conclusion that can be drawn from the characterization of these films is that the properties of reactively DC planar magnetron sputtered InN films do not vary

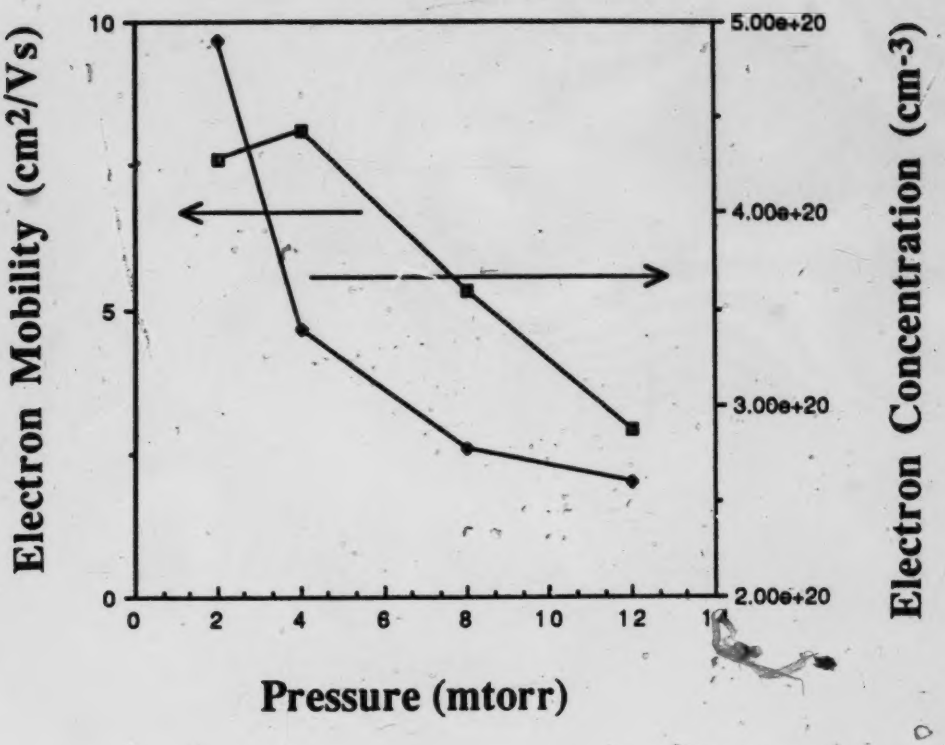

Figure A.3 Electron mobility and concentration as a function of sputter gas pressure.

significantly with deposition conditions that are typical for reactively sputtered films. This is caused by the low reactivity between the indium target and the N_2 glow discharge. To dramatically change the properties of the InN films a major departure must be made from standard sputter conditions. Tansley and Foley used such a major departure from the typical sputter conditions when they used very long deposition times (315 hours) to grow their high mobility films[3,4].